MOLECULAR AND CELLULAR BIOLOGY, Mar. 2010, p. 1303–1318 Vol. 30, No. 6
0270-7306/10/$12.00 doi:10.1128/MCB.01101-09

Mitochondrial p32 Protein Is a Critical Regulator of Tumor Metabolism via Maintenance of Oxidative Phosphorylation▽

Valentina Fogal,[1] Adam D. Richardson,[1] Priya P. Karmali,[1] Immo E. Scheffler,[3] Jeffrey W. Smith,[1] and Erkki Ruoslahti[1,2]*

Cancer Research Center, Burnham Institute for Medical Research, 10901 N. Torrey Pines Rd., La Jolla, California 92037[1]; Vascular Mapping Center, Burnham Institute for Medical Research at UCSB, 1105 Life Sciences Technology Bldg., University of California, Santa Barbara, Santa Barbara, California 93106-9610[2]; and Division of Biology, Molecular Biology Section, University of California, San Diego, La Jolla, California 92093-0322[3]

Received 17 August 2009/Returned for modification 20 September 2009/Accepted 16 November 2009

p32/gC1qR/C1QBP/HABP1 is a mitochondrial/cell surface protein overexpressed in certain cancer cells. Here we show that knocking down p32 expression in human cancer cells strongly shifts their metabolism from oxidative phosphorylation (OXPHOS) to glycolysis. The p32 knockdown cells exhibited reduced synthesis of the mitochondrial-DNA-encoded OXPHOS polypeptides and were less tumorigenic *in vivo*. Expression of exogenous p32 in the knockdown cells restored the wild-type cellular phenotype and tumorigenicity. Increased glucose consumption and lactate production, known as the Warburg effect, are almost universal hallmarks of solid tumors and are thought to favor tumor growth. However, here we show that a protein regularly overexpressed in some cancers is capable of promoting OXPHOS. Our results indicate that high levels of glycolysis, in the absence of adequate OXPHOS, may not be as beneficial for tumor growth as generally thought and suggest that tumor cells use p32 to regulate the balance between OXPHOS and glycolysis.

Tumors can be distinguished from their nonmalignant counterparts by specific molecular signatures expressed in malignant cells and tumor vasculature. We explore such differences by identifying tumor-homing peptides from phage libraries that we screen *in vivo* (60). We recently showed (19) that the cellular receptor for one of our tumor-homing peptides is a protein variously known as p32, p33, gC1q receptor (gC1qR), or hyaluronic acid binding protein 1 (HABP1). This protein was originally isolated based on its copurification with the nuclear splicing factor SF-2 (37). However, it was subsequently shown to bind also the globular heads of complement component C1q (23), hyaluronic acid (10), and numerous other extracellular and intracellular proteins (24, 28, 33, 42). Most recently it has been shown that p32 interacts with the long and short forms of the tumor suppressor ARF (30, 56, 57). Despite the numerous reports on p32 interaction partners, the role of these binding activities in the physiological function of the protein is unknown, and some investigators have proposed that p32 may be a chaperone protein (58, 65).

The p32 protein is primarily localized in the mitochondrial matrix (12, 46, 48) but has also been reported to be present in other subcellular locations (53). Some of the p32 protein can be at the cell surface, a location that appears to be specific for tumors (19). In this regard, p32 is similar to some other intracellular proteins that are also partially localized at the cell surface in tumor cells (8, 49). In addition to the partial cell surface localization of p32, many human tumors exhibit higher p32 expression levels than their nonmalignant counterpart tissues (7, 19, 52, 59). Moreover, p32 is differentially expressed during the progression of epidermal carcinoma, accumulating in metastatic islands (25).

We set out to modulate p32 expression in tumor cells to gain information on the role of this protein in cancer. We show here that p32 knockdown cells shift their metabolism from oxidative phosphorylation (OXPHOS) toward glycolysis and become poorly tumorigenic. These changes could be reversed by restored expression of p32. These results show that p32 supports oxidative phosphorylation in human cancer cells and opposes the shift of tumor cell metabolism toward glycolysis. The unique expression pattern of p32 in tumors and its crucial role in tumor metabolism make p32 a promising target for tumor therapy. The fact that this protein is upregulated in tumors and counteracts glycolytic metabolism suggests that the role of the Warburg effect in tumor growth may not be as straightforward as is generally thought.

MATERIALS AND METHODS

Reagents and cell lines. Mouse monoclonal anti-p32 (clone 60.11) and anti-β-actin antibodies were from Millipore (Temecula, CA). Monoclonal antibodies specific for OXPHOS complex I (30-kDa and 20-kDa subunits; clones 3F9 and 20E9), complex II (70-kDa subunit; clone 2E3), complex III (core I; clone 16D10), complex IV (subunits I and II; clones 1D6 and 12C4), and complex V (α subunit; clone 7H10) were from Molecular Probes/Invitrogen. Polyclonal antibody anti-p32 NH_2 terminal was described elsewhere (19). Monoclonal antiporin was from MitoSciences (Eugene, OR), and antitubulin was from Sigma. Polyclonal anti-PKM2 is from Cell Signaling (Danvers, MA).

MDA-MB-435 cancer cells (for updates on their origin refer to http://dtp.nci.nih.gov/docs/misc/common_files/cell_list.html), MDA-MB-231 breast carcinoma cells, and MDA-MB-231 D3H2LN and MCF10A-CA1a cancer cells were maintained in Dulbecco's modified Eagle medium (DMEM) supplemented with 10% fetal bovine serum (FBS) and 1% glutamine Pen-Strep solution (Omega Scientific) at 37°C and 5% CO_2. MDA-MB-231-luc-D3H2LN cells are luciferase labeled and derived from parental MDA-MB-231 cells which spontaneously metastasized to the lymph node from an orthotopic tumor (Xenogen, Alameda, CA). MCF10A-CA1a cells are fully malignant and metastatic cells derived from

* Corresponding author. Mailing address: Burnham Institute for Medical Research at UCSB, Bio II, Rm. #3119, University of California, Santa Barbara, Santa Barbara, CA 93106-9610. Phone: (805) 893-5327. Fax: (805) 893-5805. E-mail: ruoslahti@burnham.org.

▽ Published ahead of print on 25 January 2010.

premalignant human breast epithelial MCF10AT cells (61). Normal human mammary epithelial cells (HMEC) (Lonza, Walkersville, MD) were grown in MEGM Bulletkit (Lonza, Walkersville, MD).

Generation of stable cell lines. p32-deficient lines were obtained through the BLOCK-iT lentiviral RNA interference (RNAi) expression system (Invitrogen) according to the manufacturer's instructions. The optimal p32 short hairpin RNA (shRNA) sequence targets nucleotides 5′-GGATGAGGTTGGACAAGA AGA-3′ (Gene-Bank accession no. NM_001212). Control shRNA is a 2-base-pair mismatched shRNA targeting a different region of p32 cDNA (5′-CCCAA TaTCGTGGTTGAtGTTATAA-3′; lowercase, underlined nucleotides indicate the base pair mismatch). Tumor cells were transduced with p32 and control RNAi lentiviral stocks. Selection of stably transduced clones was done in medium containing blasticidin (5 μg/ml; Invitrogen). To produce a p32 construct resistant to the selected shRNA, the QuikChange II site-directed mutagenesis kit (Stratagene, Cedar Creek, TX) was used to introduce two silent mutations within the p32 sequence targeted by the shRNA (5′-GGATGAGGTTGGACAgGAgGA-3′; lowercase, underlined nucleotides indicate silent mutations). The resulting construct was transfected into an MDA-MB-435 cell clone stably expressing the p32 shRNA, and Zeocin (600 μg/ml; Invitrogen) was used to select clones with restored p32 expression.

MDA-MB-231 D3H2LN cells and human mammary epithelial cells stably expressing p32 were produced using the lentiviral vector pCDH1-MCS1-EF1 Puro (System Biosciences, Mountain View, CA) and selected with puromycin (Sigma) (1 μg/ml).

Quantification of growth rates and cell death. MDA-MB-435 clones were seeded in DMEM (25 mM glucose)–10% dialyzed FBS in triplicate at a density of 2.5×10^4 cells per well in 12-well plates and allowed to adhere overnight. The medium was removed by washing and replaced with glucose-free DMEM supplemented with 10% dialyzed FBS and either 25 or 2.5 mM glucose (Mediatech, Inc., Herndon, VA). The cell number in each well at each time point was quantified by flow cytometry using CountBright absolute counting beads (Molecular Probes/Invitrogen). To quantify cell death, cells were grown for 3 days in either 25, 2.5, or 0.5 mM glucose and the annexin V-fluorescein isothiocyanate (FITC) kit from BioVision (Mountain View, CA) was used to quantify dead cells by flow cytometry.

Quantification of lactate, glucose, ATP, and oxygen. Lactate and glucose concentrations in the cell media were determined using lactate (K607-100) and glucose (K606-100) assay kits from BioVision. Cellular ATP levels were determined via the ATP bioluminescence assay kit CLS II (Roche, Indianapolis, IN), while oxygen consumption by cells in culture was measured using the BD oxygen biosensor systems (OBS) from BD Bioscience. Glucose consumption/well at time T_x was calculated as (nmol glucose in media only at T_0 − nmol glucose in cell media at T_x)/cell number at T_x, where T_0 is time zero. For oxygen consumption measurements, triplicate samples of 12,000 cells seeded onto 96-well OBS plates in a final medium volume of 200 μl were used for the measurement. The number of cells was determined at each time point by sampling cells seeded into side-by-side plates. Fluorescence was measured from the bottom of the well every 24 h on a Spectra Max Gemini plate reader (excitation at 485 nm and emission at 630 nm). Each measurement was normalized by factoring in a blank reading from the same well prior to the addition of the cells and the number of cells in the well at the time of the measurement (27).

[U-^{13}C]glucose cell labeling and metabolite analysis by NMR. Metabolic flux mapping was performed according to published methods (75). In particular, 2×10^8 cells were harvested and cell metabolites were extracted twice with cold aqueous methanol. Following centrifugation (13,000 × *g*, 10 min) the supernatants were combined and evaporated to dryness. This extract was dissolved in 650 μl of D_2O (99.9% enriched; Cambridge Isotope Laboratories) and filtered through a 0.2-μm-pore-size filter for nuclear magnetic resonance (NMR) measurements. NMR experiments were performed at 30°C and 500 MHz on a Avance 500 spectrometer (Bruker, Karlsruhe, Germany). Two-dimensional [^{13}C, ^{1}H] heteronuclear single quantum coherence (HSQC) spectra were obtained using a standard gradient-based sequence. The acquisition parameters were as follows: $t_{1\max}$ = 183 ms, $t_{2\max}$ = 157 ms; data sizes were 3,072 points at t_1 and 1,024 points at t_2. Sweep width was 80 ppm, and the carrier position was 50 ppm for ^{13}C. The ^{13}C-^{13}C scalar coupling fine structures were extracted from the cross sections taken along the ^{13}C axis in an HSQC spectrum by using the Bruker XWINNMR software. After manual baseline correction, the individual multiplet components of the scalar coupling fine structures were integrated to quantify the relative contributions of singlet, doublet, and quartet signals. Measurement of total peak volumes was accomplished using Sparky (T. D. Goddard and D. G. Kneller, SPARKY 3, University of California, San Francisco).

Isolation of mitochondria and BN-PAGE. Mitochondria were isolated using differential centrifugation with buffers from a Pierce mitochondrial isolation kit according to the manufacturer's instructions. Blue native electrophoresis (BN-PAGE) of dodecylmaltoside-solubilized mitochondria was performed as described by Wittig et al. (74).

Mass spectrometry. Mass spectrometry was performed with methods described by Timmer et al. (67). The liquid chromatography/tandem mass spectrometry (LC/MS/MS) spectra were searched using Sorcerer SEQUEST (Sage-N Research) on the target-decoy ipi.HUMAN.v3.22 database. The search results were filtered and statistically analyzed by using comprehensive proteomics data analysis software Trans-Proteomic Pipeline (TPP) v4.0 JETSTREAM, revision 2, from the Institute of System Biology (ISB) and PeptideProphet/ProteinProphet (ISB), with minimum probability scores for proteins and peptides set to 0.99 and 0.9, respectively, to assure a false-positive rate of 0.02 or less. The relative abundance of each identified protein in different samples was analyzed as previously described (3).

Mitochondrial enzyme assays. The activities of respiratory chain complexes I and IV were assayed with kits (MS-130 and MS-443) from MitoSciences according to the manufacturer's instructions. Pyruvate dehydrogenase (PDH) activity was quantified with the MitoSciences kit MSP30 according to the manufacturer's instructions.

^{35}S *in vivo* labeling. Prior to labeling, cells were incubated for 1 h at 37°C in DMEM without L-methionine or L-cysteine–10% dialyzed FBS, in the presence or absence of 100 μg/ml emetine dihydrochloride hydrate (Sigma) and/or 200 μg/ml chloramphenicol (VWR). Fresh medium, with or without protein synthesis inhibitors as above, containing 60 μCi of EasyTag EXPRESS^{35}S protein labeling mix (PerkinElmer) was added to the cells and incubated for 1 h 30 min at 37°C prior to cell lysis in radioimmunoprecipitation assay (RIPA) buffer or mitochondrial isolation.

Phylogenic profiling. For phylogenic profiling we used the recently identified MitoCarta, a collection of 1,098 mitochondrial genes, and a MitoCarta phylogenic matrix containing homologs of mouse MitoCarta proteins in 500 fully sequenced species (51). Comparison of the p32 sequence with a complete nonredundant database of available protein sequences indicated that p32 is eukaryote specific. "Eukaryotic only" proteins were extracted from the matrix and hierarchically clustered several times using different distance measures (Pearson correlation, Euclidean distance, and Manhattan distance) and two different clustering techniques (McQuitty method or weighted pair group method using arithmetic averages [WPGMA] and unweighted pair group method using arithmetic averages [UPGMA] or average distance and complete linkage) (4, 32).

Preparation of micelles encapsulating rotenone. Rotenone (Sigma) dissolved in chloroform was added to a solution of 1,2-distearoyl-*sn*-glycero-3-phosphoethanolamine (DSPE)–polyethylene glycol 2000 (PEG 2000)-monomethyl ether (OMe) (Genzyme Pharmaceuticals) in chloroform at a drug/lipid mole ratio of 0.3:3. The solvent was evaporated with a thin film of moisture-free nitrogen gas. The dried lipid film thus obtained was hydrated with phosphate-buffered saline (PBS; pH 7.4) for 1 h at 60°C. The vial was then briefly vortexed and occasionally sonicated in a bath sonicator (Branson 1510) to produce a clear micellar solution incorporating rotenone. Control micelles were composed of only DSPE-PEG 2000-OMe at the same concentration as in rotenone-containing micelles.

Mice and tumors. To produce tumors, 2×10^6 MDA-MB-435 and MDA-MB-231-luc-D3H2LN cells in 100 μl of PBS were injected subcutaneously or into the mammary fat pads of female nude mice. Tumor volume was calculated using the equation volume (mm^3) = $d^2 \times D/2$, where d and D are the smallest and biggest tumor diameters, respectively. For *in vivo* bromodeoxyuridine (BrdU) labeling, tumor-bearing mice were intraperitoneally injected with 1 mg of BrdU (Sigma-Aldrich). Twenty-four hours later the tumors were removed and fixed in Bouin's solution (Ricca Chemical Company, Arlington, TX) for 72 h prior to processing for paraffin embedding.

For experimental metastasis studies 2×10^5 MDA-MB-231-luc-D3H2LN cells in 100 μl PBS were seeded into the hearts of Harlan BALB/c athymic nude mice by intracardiac injections. Metastatic bioluminescence signals were imaged every week for a total of 3 to 4 weeks using an IVIS imaging system (Xenogen, Alameda, CA) and quantified as photons per second per square centimeter with Living Image software (Xenogen). All animal experimentation received approval from the Animal Research Committee of Burnham Institute for Medical Research.

Statistical analysis. Data are expressed as means ± standard deviations (SD) for *in vitro* experiments and as means ± standard errors of the means (SEM) for *in vivo* experiments. The two-tailed Student *t* test was used for all statistical analysis. GraphPad Prism and Excel were used for statistical calculations.

Significant differences are indicated using the standard Michelin Guide scale ($P < 0.05$, significant; $P < 0.01$, highly significant; $P < 0.001$, extremely significant).

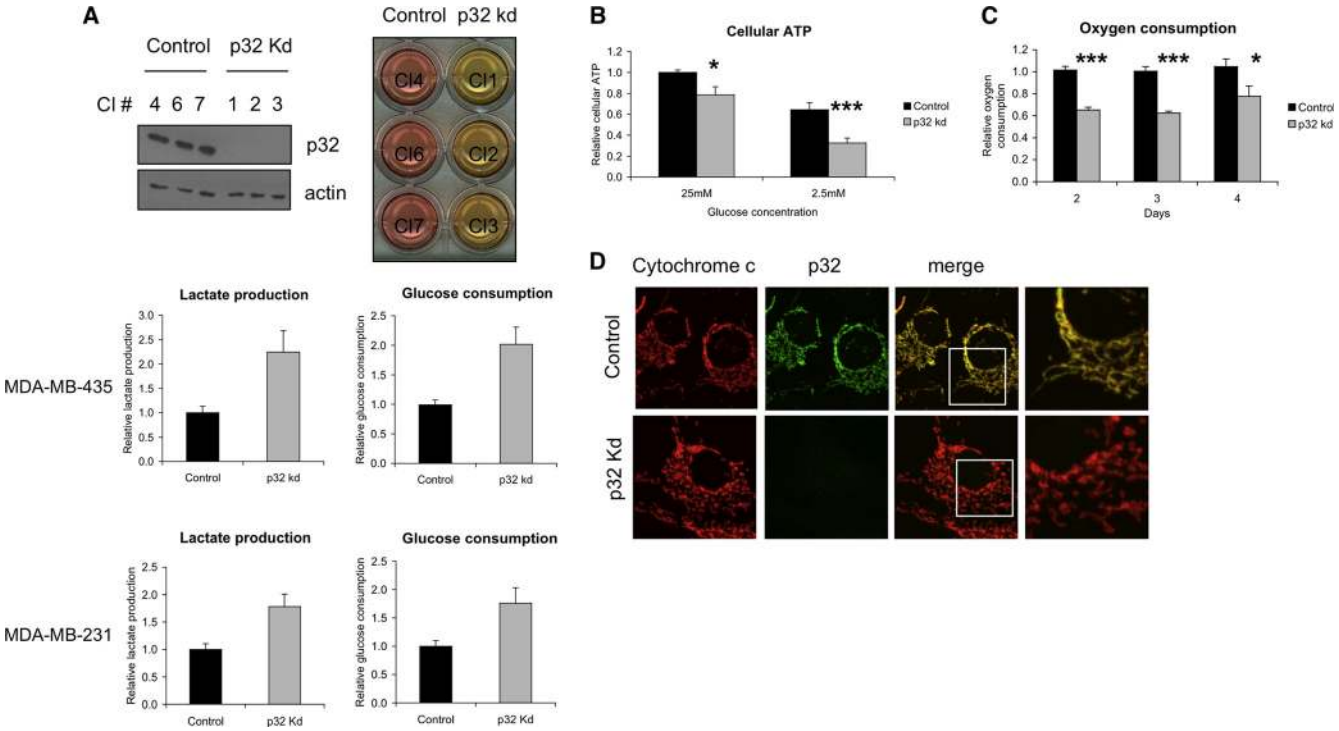

FIG. 1. Knockdown of p32 in MDA-MB-435 tumor cells. (A, top left) Immunoblot analysis on whole-cell lysates from three MDA-MB-435 clones (Cl) stably expressing shRNA for p32 (p32 knockdown [Kd] clones 1, 2, and 3) and three clones expressing a base mismatch control shRNA (control clones 4, 6, and 7). (Top right) Acidification of the culture media in p32 knockdown clones, as indicated by the color change of the phenol red indicator in the media to orange/yellow. (Bottom) Lactate production and glucose consumption 4 days after cell seeding, calculated as described in Materials and Methods and shown relative to control ($P < 0.001$). (B) Cellular ATP from lysates of p32 knockdown and control cells grown for 4 days in media with the indicated glucose concentrations. The ATP present in each lysate was normalized for the ATP production of control clones grown in 25 mM glucose. The results are the averages (±SD) of three independent experiments performed with three p32 Kd and three control clones. *, $P < 0.05$; ***, $P < 0.001$. (C) Oxygen consumption. Shown are the values for p32 knockdown clones relative to control clones. The results come from three independent experiments (±SD) performed in triplicate. ***, $P < 0.001$; *, $P < 0.05$. (D) Confocal analysis of p32 localization in cells. p32 knockdown and control cells were stained for p32 and anti-cytochrome *c*. The panels on the right are high-magnification images of the white-framed areas in the merge panels.

RESULTS

Stable knockdown of p32 alters tumor cell metabolism. To delineate the role of p32 in tumors, we expressed shRNAs complementary to p32 or a 2-base-pair mismatch control shRNA in MDA-MB-435 tumor cells. Three p32 shRNA clones, with undetectable p32 expression, and three control shRNA clones were selected for analysis (Fig. 1A). Strikingly, p32 knockdown induced acidification of the culture medium, as indicated by a phenol red color change 3 to 4 days after cell seeding (Fig. 1A). Consistent with a decrease in pH, lactate production was significantly increased in p32 knockdown cells compared to control cells (Fig. 1A).

Lactic acid is a by-product of glycolysis and accumulates under anaerobic conditions and during mitochondrial dysfunction. Reliance on glycolysis for ATP production is associated with a high rate of conversion of glucose to lactate and a high rate of glucose uptake. We found that p32 knockdown cells consumed more glucose than the control clones, indicating increased glycolysis (Fig. 1A). However, the elevated glycolytic rate and lactate production did not translate into increased cell growth of the p32 knockdown cells, as these cells grew more slowly than the control cells (see Fig. 3). Similar results were found with the breast cancer cell line MDA-MB-231 (Fig. 1, bottom).

The p32 protein is present in each of the main cellular compartments, but it is predominantly a mitochondrial protein. Consistent with a mitochondrial role for p32, a growth defect in *Saccharomyces cerevisiae* lacking the p32 homolog has been linked to an abnormality in maintaining mitochondrial ATP synthesis (48). The p32 knockdown cells, when grown in normal media containing high (25 mM) glucose, produced up to 20% less total ATP than control cells (Fig. 1B). The decrease in mitochondrial ATP production could have been greater than that, as increased ATP production via glycolysis may have compensated for reduced mitochondrial ATP synthesis. Reducing glucose concentration in the media to 2.5 mM was more detrimental to cellular ATP production in p32 knockdown cells (50% reduction) than in control clones. These data suggest that p32 may be required for efficient ATP production through oxidative phosphorylation. Consistent with such a role, p32 knockdown cells consumed less oxygen than control clones (Fig. 1C). Thus, loss of p32 shifts energy metabolism toward glycolysis, likely via perturbation of mitochondrial function. These results parallel the changes observed in

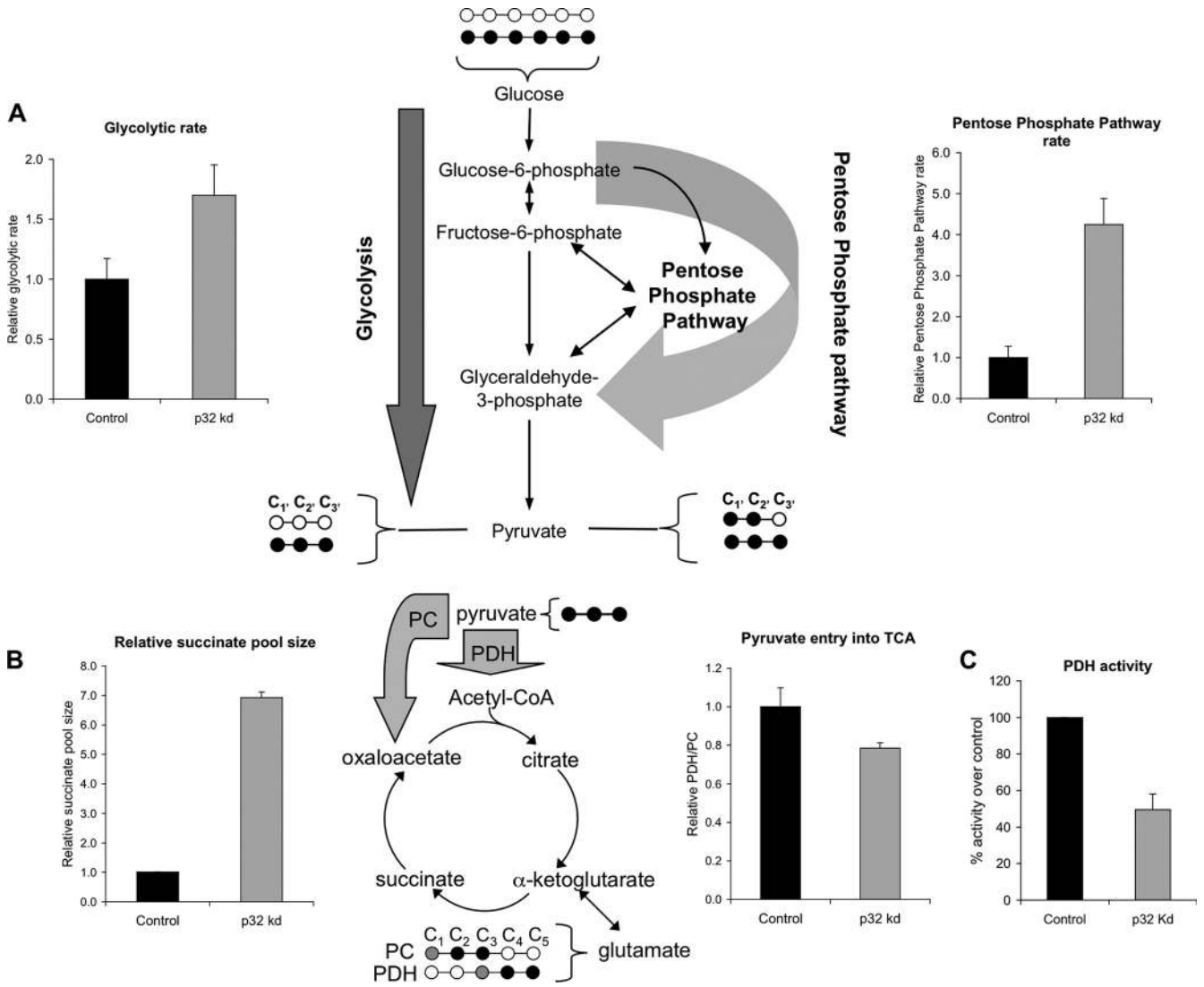

FIG. 2. Effect of p32 knockdown (kd) on central carbon metabolism. The relative flux through the Embden-Meyerhof pathway (A, left) and the pentose phosphate pathway (A, right) and into the TCA cycle (B) was determined by [U-^{13}C]glucose tracking and isotopomer analysis. Results are reported as the SD of triplicate integrations. (A) The ^{13}C labeling pattern of alanine was used to determine glycolysis and PPP. Examples of labeling patterns are shown for glucose and pyruvate, where the open circles represent ^{12}C and the filled circles represent ^{13}C. Flux of glucose through glycolysis produces pyruvate that is either uniformly ^{12}C or ^{13}C labeled, while the rearrangements of the pentose phosphate pathway result in the loss of label at C-3. (B) Effect of p32 knockdown on TCA cycle entry and flux. Pyruvate can enter the TCA cycle through either pyruvate dehydrogenase (PDH) or pyruvate carboxylase (PC), which results in different patterns of glutamate labeling (gray circles represent either ^{12}C or ^{13}C). Determining the ratio of ^{13}C at C-4 versus C-3 yields the ratio of PDH activity to PC activity. Knockdown of p32 results in a shift of pyruvate flux from PDH to PC (right graph). The relative level of succinate in each cell line was determined by integrating the peak volumes of succinate carbons C-3 and C-4 compared to glutamate carbons C-3 and C-4. Succinate pool size increased sevenfold following p32 knockdown (left graph). (C) Quantification of PDH enzymatic activity from control and p32 knockdown MDA-MB-435 cell lysates. The results are representative of four independent experiments and are expressed as percentages of PDH activity (±SD), with PDH activity in control cells as 100%. P was <0.001.

yeast p32 knockout cells. Disrupting the yeast gene homolog of the p32 gene causes growth retardation in glycerol but not glucose media, suggesting a role for p32 in the maintenance of mitochondrial oxidative phosphorylation (48).

Mitochondrial morphology is closely linked to energy metabolism. Enhanced respiration correlates with an interconnected mitochondrial network and enlarged crista compartment, while reduced OXPHOS and enhanced glycolysis correlate with fragmented mitochondrial and matrix expansion (1). Confocal analysis of mitochondria in p32 knockdown and control clones showed that the mitochondrial network was fragmented rather than fibrillar when p32 was not expressed (Fig. 1D).

To further examine glucose utilization in control versus p32 knockdown cells, the metabolism of [U-^{13}C]glucose, added in the culture media, was tracked by two-dimensional (2D) NMR and mass spectrometry. The metabolic fluxes through which the label is transferred from glucose into intermediary metabolites are shown in the schemes of Fig. 2. By analyzing the isotopomer populations of alanine C-2, we found that total

TABLE 1. Metabolic fluxes in MDA-MB-435 cells: control versus p32 knockdown[a]

Parameter	Value for:	
	Control cells	p32 kd[b] cells
Acetyl-CoA labeling rate (%)	15 ± 0	15 ± 1
Pyruvate labeling rate (%)	21 ± 3	24 ± 3
Pyruvate from PPP (%)	7 ± 2	17 ± 2
PC/PDH ratio (carbon entry to the TCA cycle)	0.35 ± 0.03	0.44 ± 0.02
Glycine from glucose (%)	20 ± 2	17 ± 1
Palmitate from glucose (%)	25 ± 0	27 ± 2

[a] Flux toward a given metabolite is calculated as a percentage of the total production of that metabolite from [^{13}C]glucose through the given pathway. Fatty acid composition was measured by gas chromatography-mass spectrometry and is presented as a percentage of the *de novo* synthesis of each fatty acid from [^{13}C]glucose. Values are means ± SD.
[b] kd, knockdown.

carbon flux significantly increased through both the Embden-Meyerhof pathway and the pentose phosphate pathway (PPP). The activity of each of these pathways contributes to the net increase in glycolytic activity. Intriguingly, although the flux through the Embden-Meyerhof pathway was consistently greater than the flux through the PPP, compared as mol/cell/h, the fold increase in PPP flux was greater following p32 knockdown. This indicates that the metabolic shift observed in this cell line is more complex than a shunting of glucose to lactate production.

Additionally, through analyzing the isotopomer distribution of glutamate, we observed a decrease in the relative activity of pyruvate dehydrogenase (PDH) and the tricarboxylic acid (TCA) cycle following p32 knockdown (Fig. 2B). This shift indicates that p32 knockdown reroutes cellular pyruvate away from oxidative phosphorylation and toward anabolic growth. A decrease in PDH activity was confirmed also by enzymatic assay (Fig. 2C). The decrease in respiration and TCA cycle flux was also marked by an increase in the pool size of succinate compared to that of glutamate. The labeling patterns of glutamate carbons C-3 and C-4 in both free glutamate and the glutamate-derived carbons of glutathione were nearly similar, indicating that the glutamate pool is well mixed. The labeling patterns for the control and knockdown cell lines were also identical. As glutamate is interconverted with the TCA cycle intermediate alpha-ketoglutarate, we compared the signal strength of succinate carbons C-3 and C-4 to that of glutamate carbons C-3 and C-4 to determine the relative mass of the TCA cycle. Knockdown of p32 resulted in a 7-fold increase in the relative amount of succinate, indicating that the TCA cycle flux is significantly inhibited. Taken together, these data support the view that p32 is critical for mitochondrial function and that its inactivation alters energy metabolism in favor of glycolysis. These changes are specific to p32 and not the result of a broad metabolic depression, as other key metabolic indicators were unchanged (Table 1). In particular, the overall ^{13}C labeling rates of both pyruvate and acetyl-coenzyme A (CoA) were similar, indicating that the core glucose metabolic pathways remained unchanged. The labeling rate of palmitate was also unchanged, signifying that fatty acid biosynthesis was not affected by p32. Although fatty acid oxidation was not directly observed in this study, the fact that the acetyl-CoA and fatty acid labeling rates are very similar suggests either that fatty oxidation is not present in the two cell lines or that the levels of oxidation are comparable.

Loss of p32 impairs cell growth and increases cell death. The p32 knockdown cells grew more slowly than control cells (Fig. 3A). The difference was particularly striking in medium containing only 2.5 mM glucose. Under these low-glucose conditions, the medium in the p32 knockdown cells did not become acidic, indicating that the cells were not able to carry out glycolysis at a level that would support cell growth. Similar results were obtained also with the breast tumor cell lines MDA-MB-231 and MCF10A-CA1a (data not shown).

Tumor cells have a tendency to undergo cell death under low-glucose conditions (62). We next determined whether loss of p32 would confer this trait on the MDA-MB-435 cells. The percentages of annexin V-positive cells in the p32 knockdown and control cells in high glucose media were similar, but the greater sensitivity of the knockdown cells became evident in low-glucose media (Fig. 3B).

Therefore, in cells with reduced p32 expression, glycolysis had become the major source of metabolic energy, as indicated by the fact that these cells acidify the medium at a high rate and are very sensitive to glucose concentrations.

p32 knockdown affects OXPHOS enzyme levels and activity. We next sought to investigate a possible role for p32 in the oxidative phosphorylation process. The electron transport chain system consists of 5 multisubunit enzymatic complexes formed from products of both nuclear and mitochondrial genes. To determine whether the defects in the p32 knockdown cells were in the electron transport chain, blue native electrophoresis (BN-PAGE) (74) was used to display and compare the protein compositions of OXPHOS complexes in control and p32 knockdown mitochondria. As shown in Fig. 4A, left, p32 knockdown resulted in a decrease in the levels of complexes III, IV, and V but not of complex II. In the particular conditions used we were not able to extract intact complex I. Second-dimension resolution of OXPHOS complexes by SDS-PAGE indicated a clear and reproducible difference in the intensities of several spots/subunits (Fig. 4A, right). Mass spectrometry analysis of some of these spots identified components of complexes IV, V, and I (Table 2).

In agreement with the BN-PAGE, lysates from three p32 knockdown tumor cell lines showed decreased levels of complex I, III, IV, and V subunits (Fig. 4B). No differences in the levels of expression of the complex II 70-kDa subunit or in the levels of the mitochondrial protein porin were observed, indicating that reduced expression of p32 specifically affects the levels of complexes I, III, IV, and V.

Reduced expression of OXPHOS complexes in p32-deficient cells had a direct effect on their enzymatic activity, as demonstrated for complexes I and IV, whose ability to oxidize NADH and cytochrome *c*, respectively, was significantly reduced by p32 knockdown (Fig. 4C).

To show the specificity of the shRNA knockdown, we restored p32 production in knockdown cells. We employed a p32 cDNA in which silent mutations confer resistance to inhibition by the p32 shRNA to bring p32 expression to the original level. This treatment normalized lactate accumulation and glucose consumption (Fig. 5A). It also restored OXPHOS complex

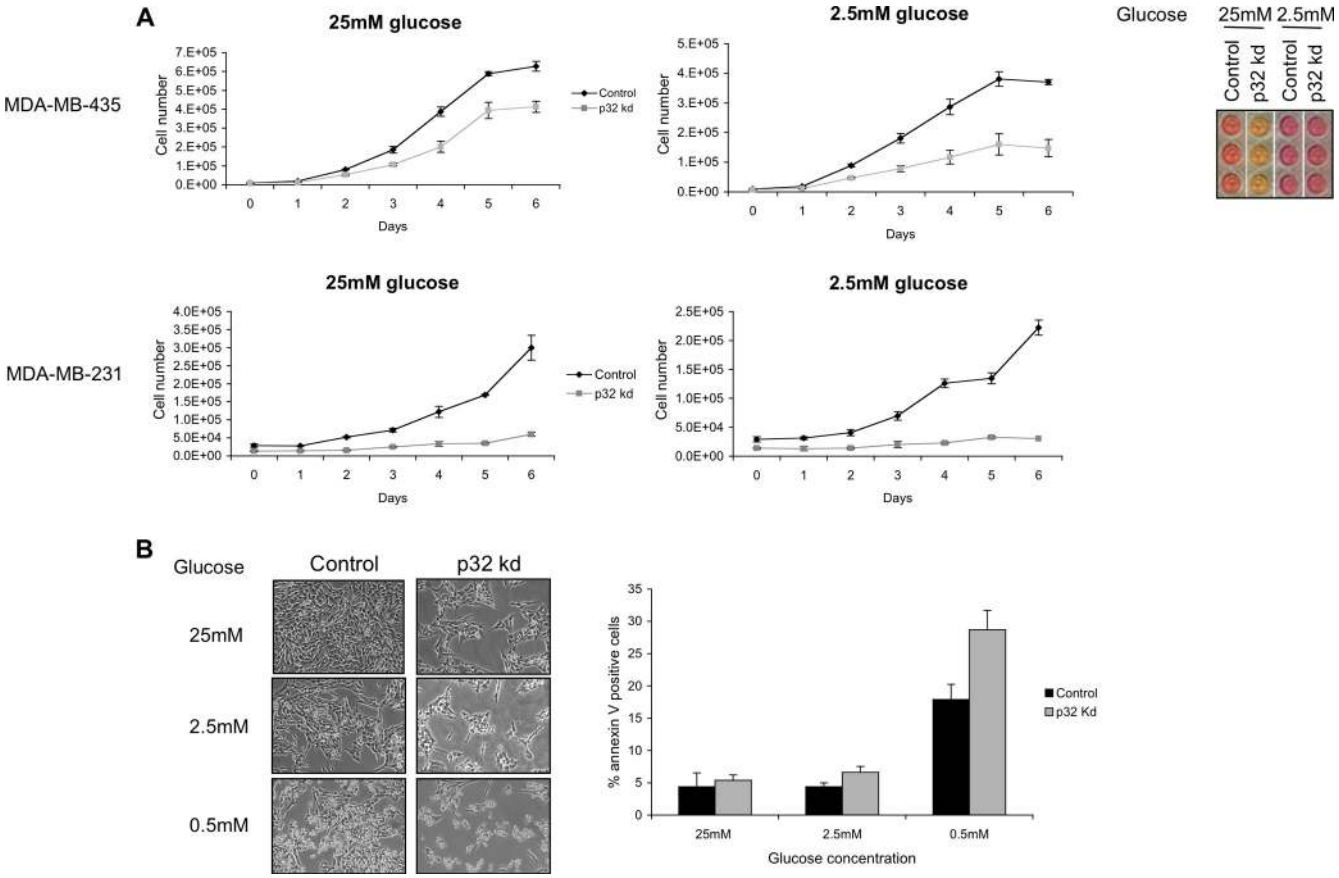

FIG. 3. Effect of p32 knockdown on growth and survival of tumor cells *in vitro*. (A) Proliferation of MDA-MB-435 and MDA-MB-231 p32 knockdown (kd) and control cells under high (25 mM)- and low (2.5 mM)-glucose conditions. Average cell number at each time point was determined by counting cells in triplicate wells of three p32 knockdown and control clones ($P < 0.001$) of MDA-MB-435 cells or a pool of clones of MDA-MB-231 cells. The right panel shows the color of media of three control and p32 kd MDA-MB-435 clones after 6 days in 25 mM or 2.5 mM glucose. (B, left) Microscopic analysis of p32 knockdown and control MDA-MB-435 cells after 3 days in medium containing the indicated glucose concentrations. (Right) Cell death was quantified by fluorescence-activated cell sorter (FACS) analysis of cells that bind FITC-annexin V ($P < 0.05$).

expression (Fig. 5B) and the proliferation rate of the knockdown cells (Fig. 5C).

To rule out the possibility that p32 regulates mitochondrial metabolism indirectly via extramitochondrial functions, we tried to rescue the knockdown phenotype with a cytoplasmic form of p32. Human p32 is expressed as a proprotein of 282 amino acids (aa) whose first 73 amino acids, containing a mitochondrial localization signal, are required for localizing the protein to the mitochondria and are subsequently cleaved to generate mature p32 (48). cDNA constructs encoding a protein either lacking the first 73 aa or containing an N-terminal hemagglutinin (HA) tag produced a cytoplasmic-only p32 (Fig. 6A). However, the expression levels of these constructs were significantly lower than those of the wild-type p32 construct (Fig. 6B). Selected and isolated stable single-cell clones expressed no or extremely low levels of cytoplasmic p32, where the phenotype of p32 knockdown was clearly not rescued (data not shown). We were able to obtain significantly higher expression of cytoplasmic p32 constructs only upon inhibition of proteasomal degradation (Fig. 6C). These data indicate that p32 protein, unable to localize to the mitochondria, is extremely unstable.

p32 is involved in the synthesis of mitochondrially encoded proteins. Mitochondrial DNA contains 37 genes, coding for 13 polypeptides/subunits of the mitochondrial electron respiratory chain and 22 tRNAs and 2 rRNAs required for the synthesis of these polypeptides. Among the 5 respiratory chain complexes, only complex II levels were not affected by p32 knockdown. Interestingly, complex II is the only OXPHOS complex encoded exclusively by nuclear DNA. The other complexes consist of polypeptides encoded by both nuclear and mitochondrial DNA. As shown by BN-PAGE and immunoblot analysis, loss of p32 affected the expression of several polypeptides encoded in the mitochondria and nucleus (Fig. 4). However, among the mitochondrial subunits tested, p32 knockdown had a greater effect on the expression levels of the complex I 20-kDa and 30-kDa subunits and subunits I (COX1) and II (COX2) of complex IV (Fig. 4B, graph), which are all polypeptides encoded by mitochondrial DNA. It is possible that reduced levels of some mitochondrial-DNA-encoded subunits indirectly affect the amounts of other subunits. For example, deficiency of mitochondrially encoded polypeptides likely affects proper assembly of complexes I, III, IV, and V, with consequent instability/degradation of subunits encoded by the nuclear genome.

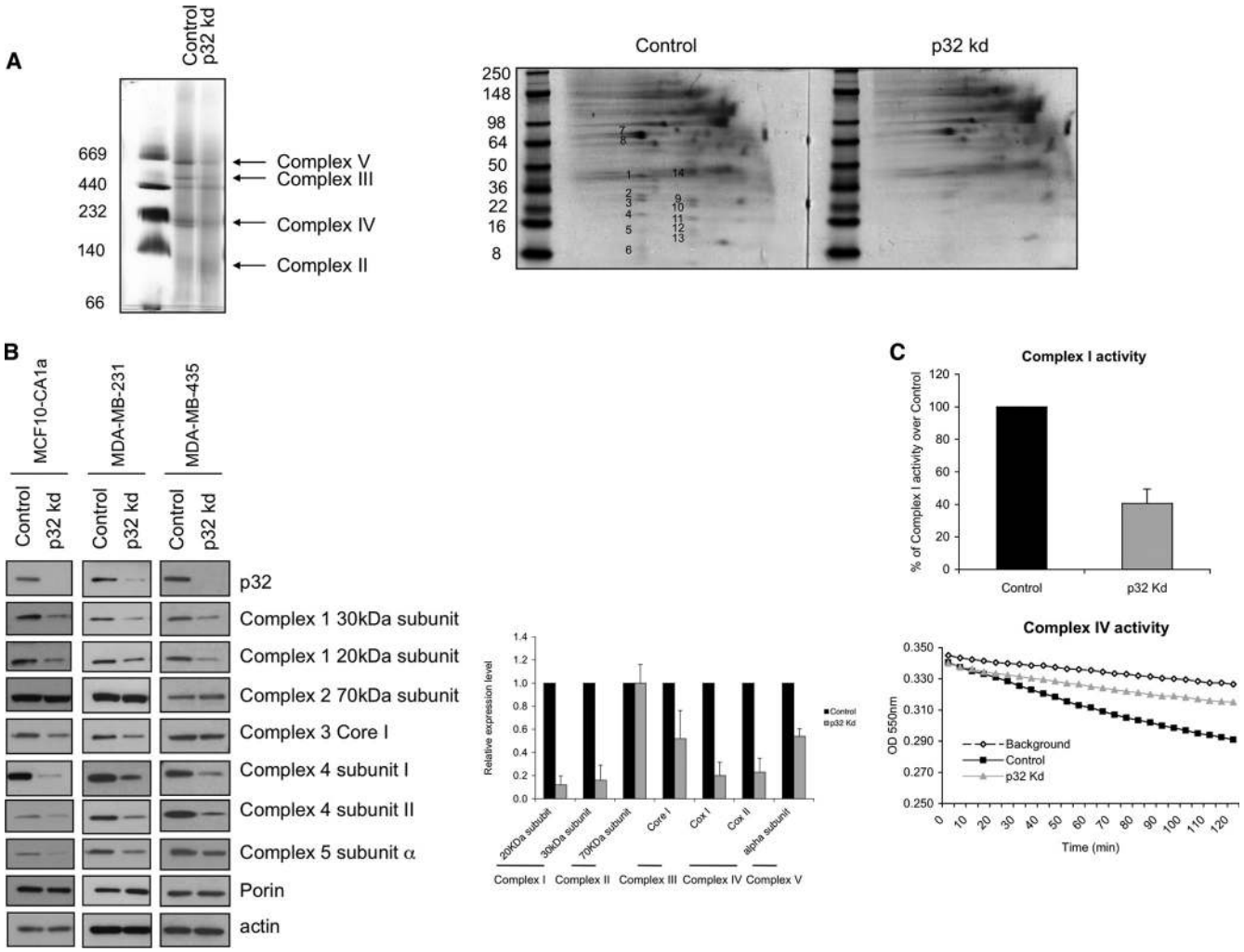

FIG. 4. p32 knockdown (kd) results in decreased protein levels of mitochondrial respiratory complexes I, III, IV, and V. (A, left) Representative BN-PAGE of dodecylmaltoside-solubilized mitochondria from control and p32 knockdown MDA-MB-435 cells. (Right) Subunits of the native complexes resolved by 1D electrophoresis were separated by SDS-PAGE. Arrows mark spots with the highest degree of downregulation upon p32 knockdown, and they have been identified by mass spectrometry (Table 1). The gel is representative of at least three independent BN-PAGE experiments. (B) Lysates from control and p32 knockdown MDA-MB-435, MDA-MB-231, and MCF10-CA1a cells were probes for various respiratory complex subunits. Porin antibody was used to test the effect of p32 knockdown on a non-OXPHOS mitochondrial protein. Actin was used as loading control. The intensities of the bands from 3 or 4 independent Western blots from MDA-MB-435 lysates were quantified by Image J software and expressed relative to controls (graph). (C) Assays of complex I and IV activity from MDA-MB-435 control/p32 knockdown lysates. Complex I activity in p32-deficient cells is expressed as % relative to control cells, and the bars represent the ranges of three independent experiments. The activity of complex IV was determined by following the oxidation of cytochrome *c* by control and p32 knockdown cell lysates. Lysis buffer only was used as the background reference measurement. The graph is representative of three independent assays, each performed in duplicate and with three different lysate concentrations. OD, optical density.

Since reduced expression of the 20-kDa and 30-kDa subunits of complex I and subunits I and II of complex IV due to p32 deficiency did not occur at the transcriptional level (Fig. 7A), we examined whether p32 plays any role in mitochondrial protein synthesis. Newly synthesized proteins were tracked by labeling cells in culture with [^{35}S]methionine. To distinguish between proteins synthesized in the cytoplasm and mitochondria, cells were pretreated with emetine and chloramphenicol, which are specific inhibitors of cytoplasmic and mitochondrial protein synthesis, respectively. Electrophoresis of whole-protein extracts from emetine-treated cells showed a few faint radioactive bands in the control but not in the p32-deficient cells (Fig. 7B). The synthesis of these proteins was completely inhibited by chloramphenicol, which suggests that they represent products of mitochondrial protein synthesis. In a second approach, the cytoplasmic and mitochondrial fractions of cells labeled in the presence or absence of emetine were analyzed. As shown in Fig. 7C, no ^{35}S-labeled proteins were found in the cytoplasm of emetine-treated cells, indicating efficient blockade of cytoplasmic protein synthesis, whereas the profile of mitochondrial proteins closely resembled the profile in whole lysates of emetine-blocked control cells (Fig. 7B). Clearly this profile reflects the products of mitochondrial protein synthesis, which was strikingly reduced in p32-deficient cells (Fig. 7C).

In an attempt to categorize p32 in a specific biological pathway, we performed phylogenic profiling, a bioinformatics tech-

TABLE 2. Mass spectrometry identification of 2D BN-PAGE gel spots[a]

Spot	Protein identification	Accession no.[b]	OXPHOS complex	Spectral counts
1	ATP synthase subunit gamma (F_1 complex)	IPI00219567		36
2	ATP synthase subunit B (F_0 complex)	IPI00029133		49
3	ATP synthase subunit 0 (F_1 complex)	IPI00007611		68
5	ATP synthase subunit F (F_0 complex), isoform 2	IPI00219291	ATP synthase (complex V)	6
6	ATP synthase subunit E (F_0 complex)	IPI00218848		5
7	ATP synthase subunit alpha (F_1 complex)	IPI00440493		150
8	ATP synthase subunit beta (F_1 complex)	IPI00303476		113
4	NADH dehydrogenase (ubiquinone) 1 alpha subcomplex 13	IPI00219685	NADH dehydrogenase (ubiquinone) (complex I)	7
10	NADH dehydrogenase (ubiquinone) 23-kDa subunit	IPI00010845		5
9	Cytochrome *c* oxidase subunit II	IPI00017510		42
11	Cytochrome *c* oxidase subunit IV, isoform 1	IPI00006579		25
12	Cytochrome *c* oxidase polypeptide Vb	IPI00021785	Cytochrome *c* oxidase (complex IV)	11
13	Cytochrome *c* oxidase polypeptide VIc	IPI00015972		15
14	Malate dehydrogenase	IPI00291006		48

[a] Gel spots indicated in Fig. 4A were processed for mass spectrometry. The spectral counts refer to the number of peptides found for each identified protein.
[b] International Protein Index (IPI) database, version 3.22.

nique in which the joint presence or absence of different proteins throughout evolution across large numbers of species is used to imply a meaningful biological connection (51, 54). p32 phylogenic analysis was performed as described in Materials and Methods, and relatively small clusters of p32-related proteins are reported in Fig. 7D. The overall results from multiple clustering approaches indicated that DAP-3 (death-associated protein 3) was phylogenetically closest to p32. Of interest,

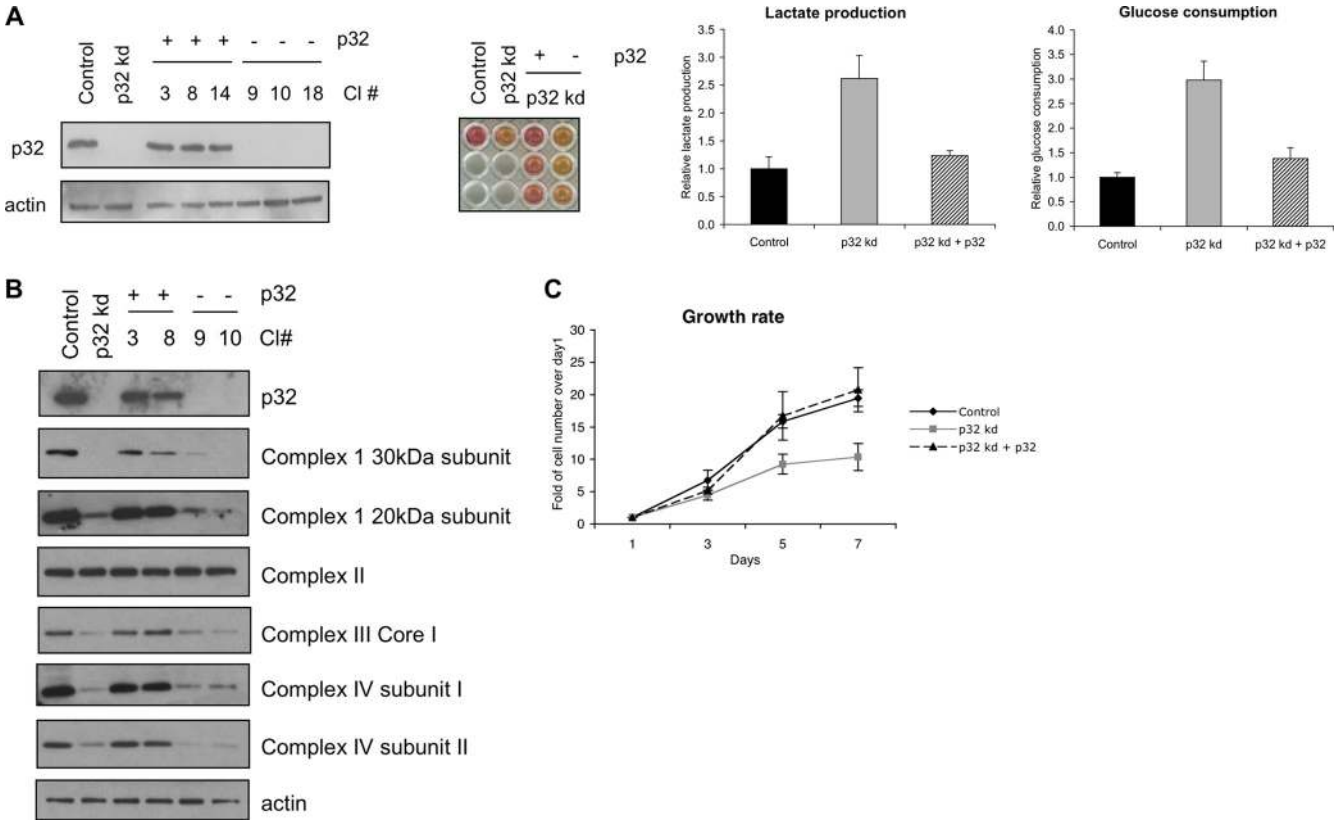

FIG. 5. Rescue of the p32 knockdown (kd) effect by restored p32 expression. (A, left) Immunoblot analysis of a parental p32 kd clone and single clones derived from it that express p32 from a cDNA resistant to p32 shRNA silencing (clones [Cl] 3, 8, and 14) or that were transfected with empty vector (clones 9, 10, and 18). A clone expressing control shRNA (control) was used to detect the endogenous level of p32. (Middle) Restoration of culture medium pH by reintroduction of p32. (Right) Graphs showing lactate production and glucose consumption in control, p32 kd, and p32-restored (p32 kd + p32) clones. (B) Western blot analysis was performed on whole-cell lysates prepared from control cells, parental p32-deficient cells, and single clones with restored (clones 3 and 8) or not restored (clones 9 and 10) p32 expression. Equivalent amounts of proteins were immunoblotted with several OXPHOS complex subunits and β-actin as the loading control. (C) Growth rate of cells with restored p32 expression versus control and p32 knockdown cells. Three single clones with restored p32 expression were tested.

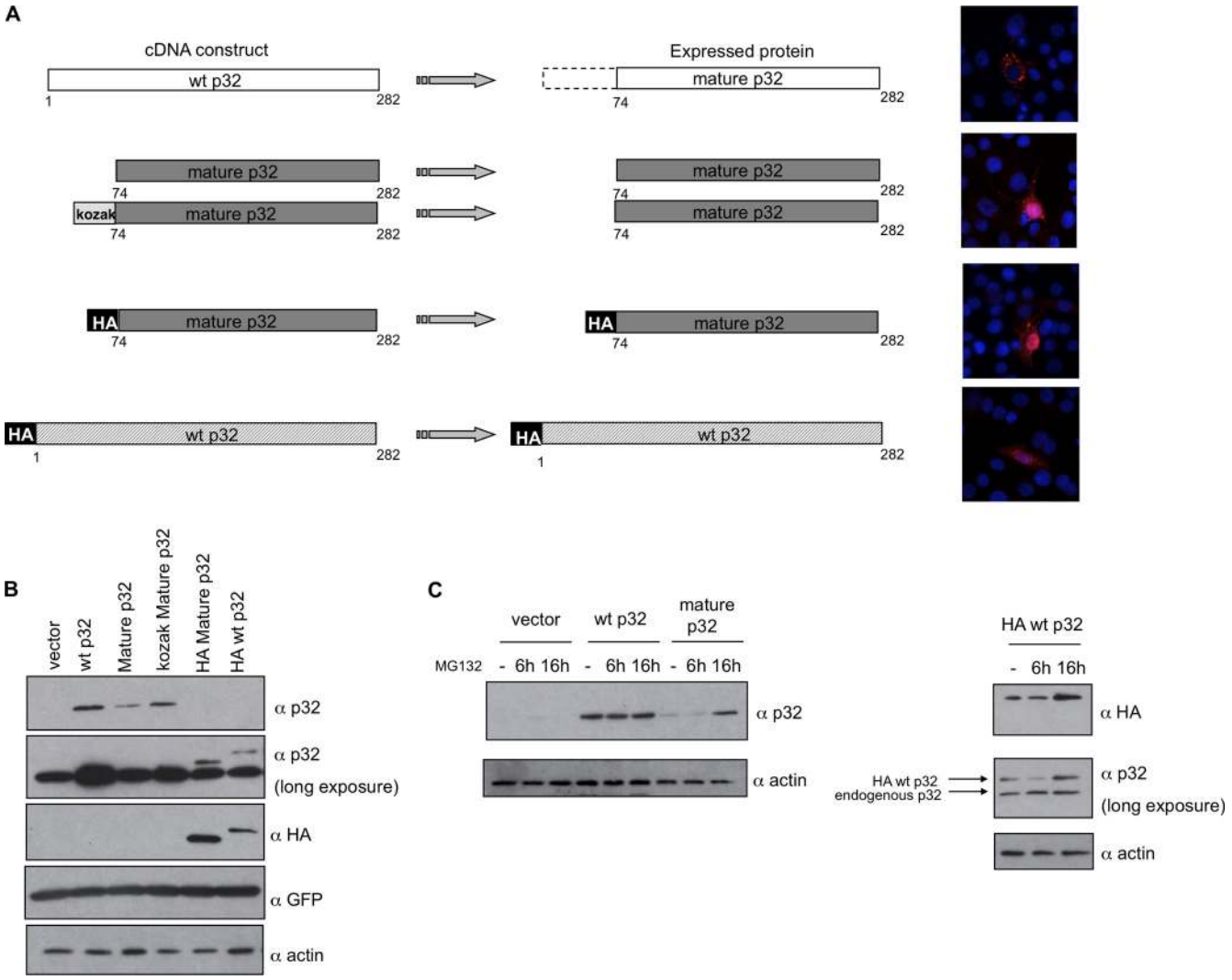

FIG. 6. Cytoplasmic p32 is unstable. (A) Schematic representation and cellular localization (images on the right) of p32 cDNA constructs and their protein products. The first 73 amino acids (aa) at the N terminus of wild-type (wt) p32 are required for mitochondrial localization of p32. Within cells p32 is present as the mature form (aa 74 to 282) after cleavage of the mitochondrial localization signal. Constructs encoding aa 74 to 282 produce only mature p32, which is unable to localize to mitochondria. Addition of an N-terminal HA tag to the full-length cDNA construct also prevents the import of p32 to mitochondria and the cleavage to the mature form. (B) The indicated p32 cDNA constructs were transiently transfected into 293 cells. At 24 to 48 h posttransfection, cell lysates were collected and the expression of p32 was analyzed by immunoblotting. Constructs encoding p32 protein unable to localize within the mitochondria are expressed at significantly lower levels than constructs encoding wt p32. Introduction of a Kozak sequence upstream of the mature p32 (aa 74 to 282) cDNA did not enhance the expression level. A green fluorescent protein-encoding construct was cotransfected to check transfection efficiency. α, anti. (C) Treatment of the transfected cells with the proteasome inhibitor MG132 (20 μM for 16 h) significantly increased the levels of cytoplasmic p32, indicating that unprotected cytoplasmic p32 is rapidly degraded.

DAP-3 has been previously implicated in both mitochondrial protein synthesis and apoptosis (6). *dap3* gene ablation results in an embryonic-lethal phenotype, associated with aberrant mitochondrial morphology and reduced production of proteins encoded by the mitochondrial genome. Similar to p32 knockdown, loss of DAP-3 expression results in significant impairment of respiration (36), and its overexpression has been reported in some invasive cancers (45).

p32 is involved in tumor maintenance and malignancy. It appears that p32 is required to sustain tumor cell growth by maintenance of respiration and oxidative phosphorylation. To assess whether the mitochondrial effect of p32 is specific to the transformed state, we investigated the impact of p32 overexpression on the energy metabolism of normal cells. As shown in Fig. 8A, overexpression of p32 in human mammary epithelial cells did not enhance OXPHOS, since levels of complex I and IV activity and the total amount of cellular ATP were unchanged. The increased p32 levels and the corresponding metabolic shift in tumor cells may represent a tumor cell-specific rewiring of a normal metabolic pathway. Aerobic glycolysis even in the presence of oxygen (the Warburg effect) is an almost universal feature of tumors, and the expression of the glycolytic enzyme pyruvate kinase isoform 2 (PKM2) is implicated in this metabolic phenotype and tumorigenesis (9). Interestingly, all the tumor cell lines used in these studies were shown to express PKM2 (Fig. 8B). Together with the above

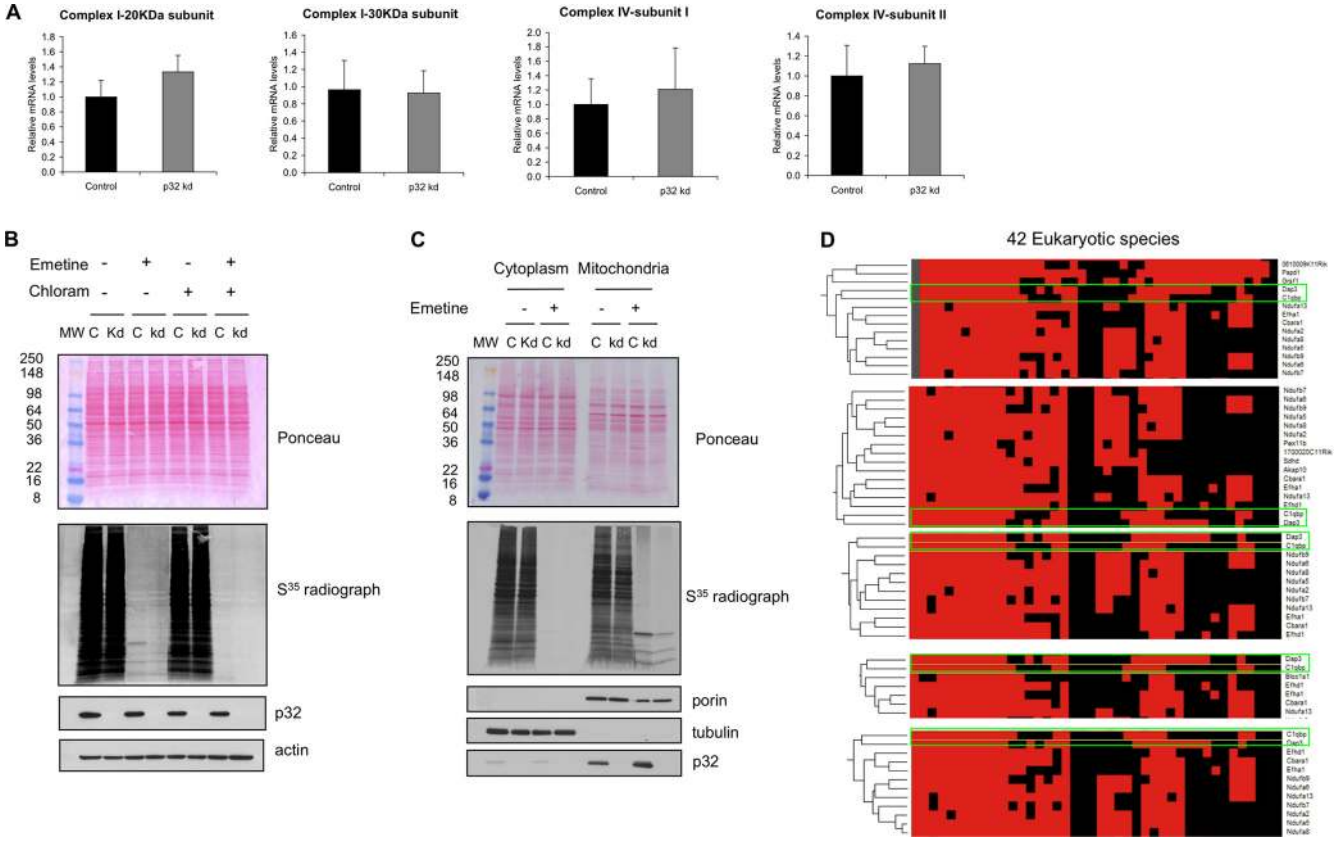

FIG. 7. p32 is involved in mitochondrial protein synthesis. (A) Quantitative PCR (QPCR) of the indicated gene transcripts from three single clones of control and p32 knockdown (kd) MDA-MB-435 cells. (B) Control and p32 knockdown MDA-MB-435 cells were labeled with [^{35}S]methionine in the presence or absence of emetine and/or cloramphenicol (Chloram). Total proteins separated by SDS-PAGE and transferred on nitrocellulose membrane were visualized by Ponceau staining (top), while newly synthesized, ^{35}S-labeled proteins were visualized by phosphorimager (middle). p32 protein was detected by Western blotting. β-Actin was used as a loading control. (C) Control and p32 knockdown MDA-MB-435 cells were labeled with [^{35}S]methionine in the presence or absence of emetine and subsequently fractionated in mitochondrial and cytoplasmic fractions. (Top) Ponceau staining of cytoplasmic and mitochondrial fractions resolved by SDS-PAGE. The ^{35}S radiograph (middle) shows newly synthesized proteins. The quality of the fractionation was checked by Western blotting with tubulin and porin, which are cytoplasmic and mitochondrial markers, respectively. (D) Identification of p32-associated proteins via phylogenic analysis. Phylogenic profiling of p32 and "eukaryote-only" MitoCarta proteins across 42 eukaryotic species is shown. Red squares indicate homology of a mouse mitochondrial protein (row) with a protein in a eukaryotic species (column). The graphs represent the mitochondrial proteins most closely related to p32, as obtained by the following clustering techniques: first (top) graph, dissimilarity, Euclidean distance; linkage rule, McQuitty's criteria; second graph, dissimilarity, Euclidean distance; linkage rule, average linkage; third graph, dissimilarity, Euclidean distance; linkage rule, complete linkage; fourth graph, dissimilarity, Manhattan distance; linkage rule, average linkage; fifth graph, dissimilarity, Manhattan distance; linkage rule, McQuitty's criteria.

results, this suggests that both elevated glycolysis and p32-dependent changes in OXPHOS are required to sustain tumorigenicity of these tumor cells. To address the role of p32 in tumorigenesis, the tumor growth of control and p32 knockdown cell clones in nude mice was monitored. The p32 knockdown cells produced either smaller tumors than controls or tumors that were swollen and soft, that were purple, and that released blood upon excision, indicating intratumoral hemorrhage (Fig. 8C). Even with the hemorrhage contributing to the size of the knockdown tumors, the growth rate of these tumors was significantly lower than that of controls ($P < 0.001$). Assessment of cell proliferation in the tumors by measuring BrdU incorporation showed significantly reduced number of BrdU-positive cells in the p32 knockdown tumors (Fig. 8D), which is consistent with the slow proliferation rate of the knockdown cells *in vitro*. Histopathological analysis of tumor sections revealed extensive necrosis in the p32 knockdown tumors compared to control tumors (Fig. 8E). The onset of tumor appearance and kinetics of tumor growth were rescued by reintroduction of p32. Tumors that originated from two p32-complemented single clones grew significantly faster than parental p32 knockdown tumors (Fig. 8F).

It is likely that impaired growth of p32 knockdown tumors is due to reduced OXPHOS activity since chemical inhibition of complex I by rotenone treatment was able to mimic the p32 knockdown phenotype *in vitro* and to a certain extent also *in vivo* (Fig. 9).

The effect of p32 overexpression on MDA-MB-435 tumor xenografts was not investigated because in this cell line we failed to obtain stable expression of p32 at levels higher than basal (Fig. 10A). However, stable overexpression of p32 was obtained in cell lines with endogenous p32 levels lower than those in MDA-MB-435 cells. In these cell lines overexpression of p32 did not affect the levels of OXPHOS subunits (Fig. 10B and data not shown).

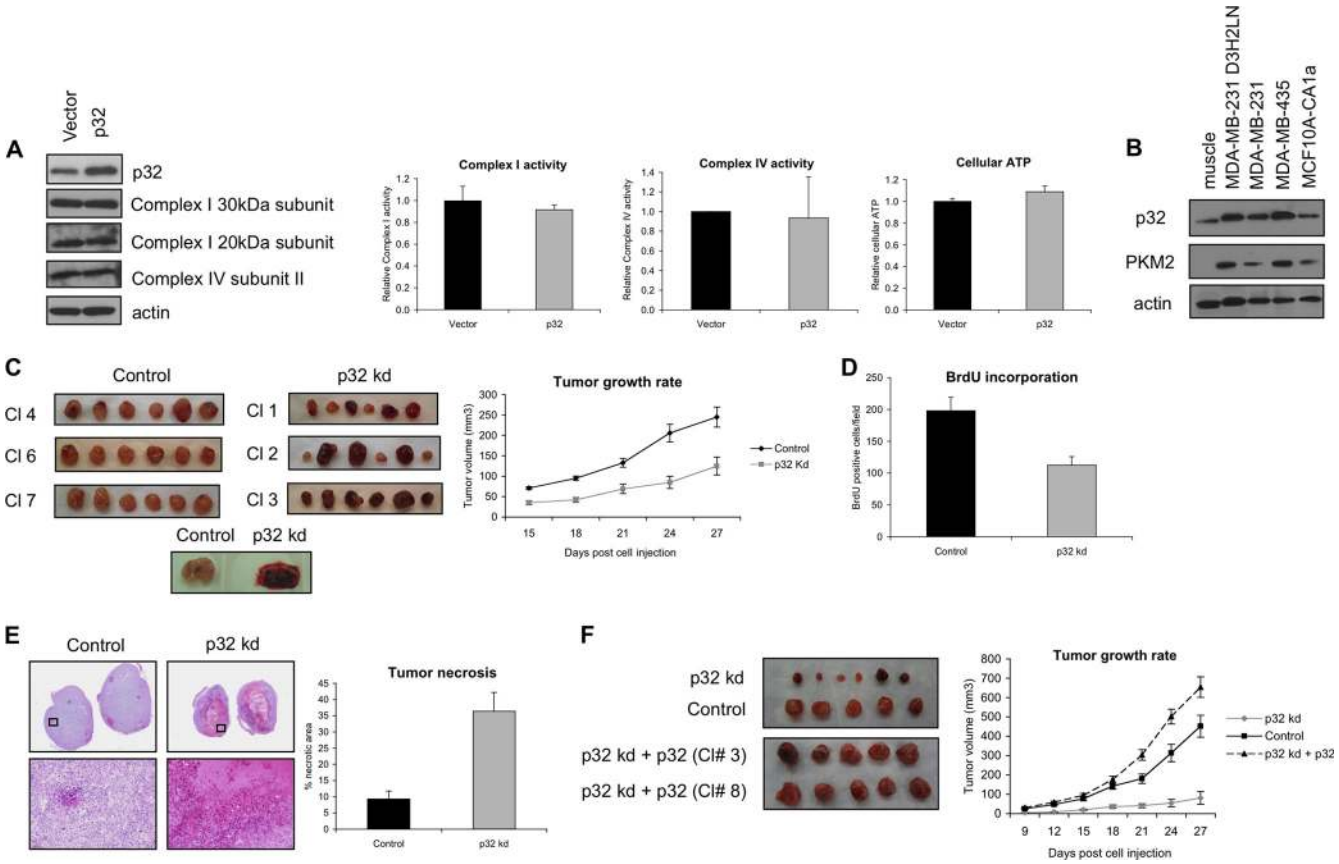

FIG. 8. Tumor growth properties and metastatic potential of p32 knockdown and p32-overexpressing cells. (A) Expression levels of the indicated OXPHOS subunits, complex I and IV activity, and total cellular ATP in normal human mammary cells stably overexpressing p32 or an empty vector. The graphs indicate averages relative to empty-vector-expressing cells (±SD) of three independent experiments. P was <0.05. (B) Immunoblotting from lysates of the indicated tumor cell lines. Mouse muscle lysate was included as a control of adult tissue negative for the expression of the PKM2 isoform. Total cell lysates were probed with polyclonal anti-p32, polyclonal anti-PKM2, and antiactin as a loading control. (C) Tumors were grown from three MDA-MB-435 p32 knockdown (kd) and control clones (6 mice per clone) in nude mice. (Left) Control tumors are homogenous in size, while p32 kd tumors are either significantly smaller than the control cell tumors or swollen and hemorrhagic. The lower panel shows an example of a knockdown cell tumor with extensive necrosis accompanied by hemorrhage. (Right) Average tumor volume as a function of time (±SEM; $P < 0.001$). (D) BrdU incorporation in tumor cells. Mice were administered a pulse of BrdU 24 h prior to sacrifice. The graph indicates the number of cells per field that scored positive for BrdU staining. The data were derived by counting via Image J software the BrdU-positive cells in 4 random fields per tumor ($n = 14$ tumors per group). P was <0.01. (E) Hematoxylin and eosin staining of tumors derived from p32 kd and control cell clones. Pink areas in p32 kd tumors are indicative of extensive necrosis. The upper images were taken with a 10× magnification, and the lower images correspond to the indicated framed areas at 200× magnification. The percentage of pink/necrotic areas was calculated via Image J software ($P < 0.001$). (F) Tumor growth properties of control cells, p32-deficient MDA-MB-435 cells, and two single clones derived from p32 knockdown cells by reintroducing p32 shRNA-resistant p32 cDNA.

Silencing of p32 in the highly aggressive MDA-MB-231 D3H2LN breast cancer cells reduced tumor development (Fig. 10C); however, stable overexpression of p32 did not accelerate tumor growth (Fig. 10C) but did enhance tumor metastatic potential, as indicated by quantification of metastatic foci formed upon intracardiac injection (Fig. 10D). Taken together, these data suggest that p32 is important for tumor maintenance and malignancy.

DISCUSSION

We show here that attenuation of p32 expression increases glycolysis while reducing cell proliferation and tumorigenesis and that restored expression of p32 rescues the original phenotype of the cells. We also provide evidence that p32 sustains mitochondrial oxidative phosphorylation by playing a role in the synthesis of mitochondrial-DNA-encoded genes. These results show that the mitochondrial p32 protein is a critical regulator of tumor metabolism and important for tumor maintenance and malignancy. Moreover, that a protein overexpressed in cancer cells supports oxidative phosphorylation provides a novel perspective on the generally held belief that increased glycolysis under aerobic conditions (the Warburg effect) promotes tumor growth.

We provide several lines of evidence to show that p32 sustains OXPHOS and that its absence increases glycolysis, while impairing cell proliferation *in vitro* and tumor growth *in vivo*. The apparent molecular mechanism that our results provide for this metabolic effect is that p32 controls the synthesis of the proteins that the mitochondrial genome contributes to the

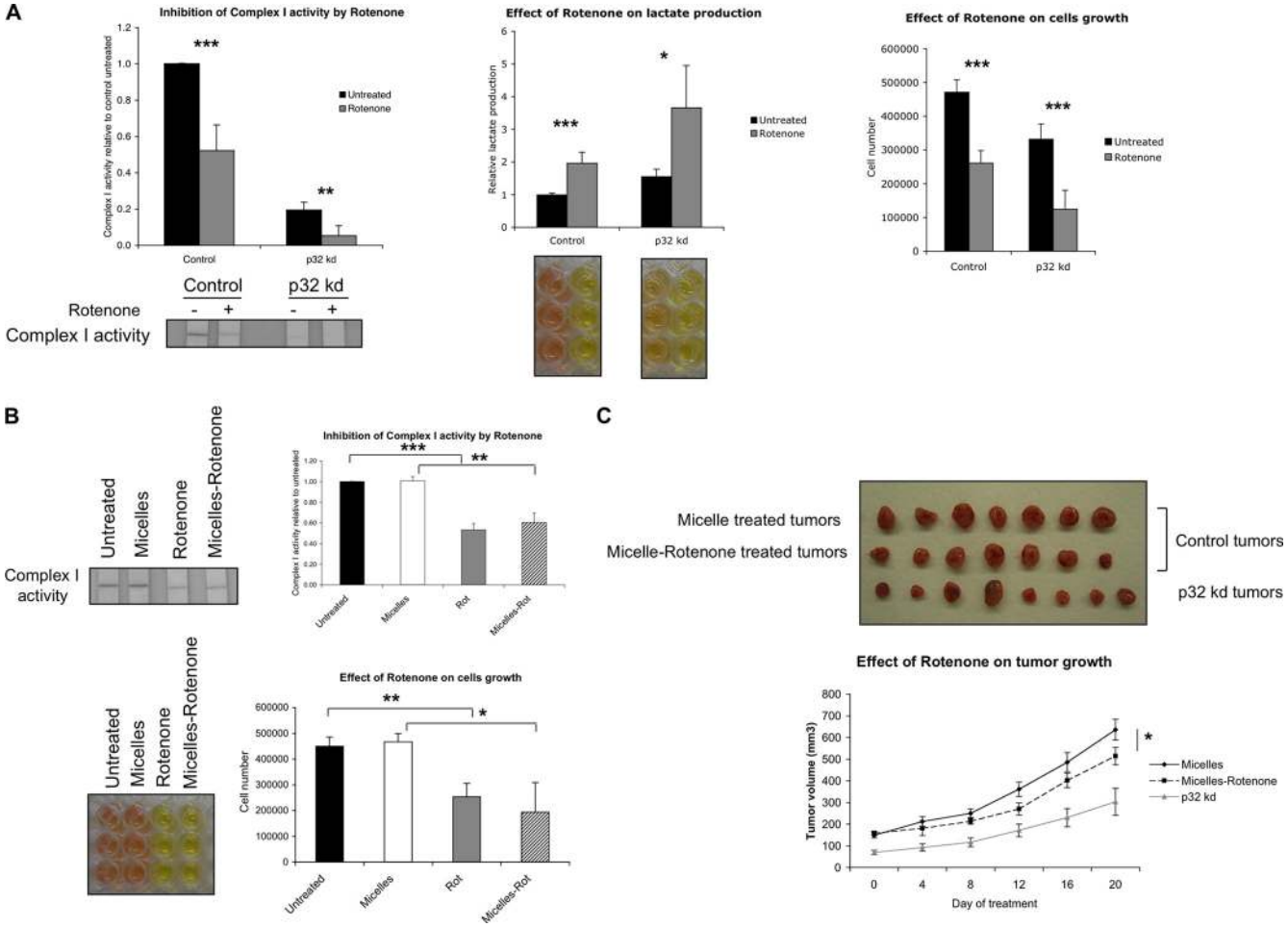

FIG. 9. Inhibition of complex I activity by rotenone treatment mimics the p32 knockdown phenotype. (A) Control and p32 knockdown (kd) MDA-MB-435 cells were treated with 100 nM rotenone for 4 days. Complex I activity was significantly reduced in both cell lines. Complex I activity is significantly lower in the p32 knockdown cells than in control cells and is almost completely eliminated in the rotenone-treated cells. The dose of rotenone used did not affect cell survival but led to cell medium acidification by enhanced lactate production (middle) accompanied by a reduced cell proliferation rate (right). (B) To investigate the effect of rotenone on tumor growth, rotenone was incorporated into micelles. Both forms of rotenone were equally effective in reducing complex I activity, increasing lactate production and reducing cell growth. Bars indicate averages ± SD of at least three independent experiments, each performed in triplicate. *, $P < 0.05$; **, $P < 0.01$; ***, $P < 0.001$. (C) Mice bearing MDA-MB-435 tumor xenografts were treated daily with 1 mg/kg of body weight micellar rotenone or an equal amount of micelles only for 20 days. The growth of p32 knockdown tumors was monitored in parallel for comparison. *, $P < 0.05$ (micelles versus micellar-rotenone-treated control tumors).

oxidative electron transfer chain. This in itself is a novel finding. The way in which p32 specifically accomplishes this trigger mechanism will be a subject of further investigation; however, it is possible that a chaperone-like function of p32 is involved.

The expression of p32 has been tied to apoptosis and autophagy via the tumor suppressor ARF (30, 56, 57), and autophagy consumes mitochondria (31, 44). However, as increasing p32 expression reportedly enhances autophagy by stabilizing the mitochondrial short form of ARF (56) and as we show that knocking down p32 increases glycolysis, it is unlikely that the effect on glycolysis would be secondary to autophagy. Furthermore, the apoptosis-promoting activity of p32 through the long form of the ARF protein requires p53 activity (30). As p53 is mutated in two of the cell lines we used, an involvement of apoptosis-related p32 activity in metabolic regulation is also unlikely. In fact, our *in vitro* and *in vivo* data present a protumorigenic function for p32 that is more consistent with the reported upregulation of p32 in tumors and that is likely linked to its role in metabolism. In support of this, our findings are consistent with earlier studies showing that depleting or reducing mitochondrial DNA levels with ethidium bromide produces cells with absent OXPHOS and a lower growth rate *in vitro* (14, 39, 73). Inhibiting mitochondrial-DNA-encoded protein synthesis in tumor cells also produces effects similar to our p32 knockdown (5, 68, 76). In addition, we obtained data showing that chemical inhibition of at least one OXPHOS complex (complex I) mimics the effect of p32 knockdown *in vitro* and at least partially *in vivo*. Collectively, we believe these findings couple p32 loss and the subsequent impaired OXPHOS with reduced tumorigenicity.

Our results on the metabolic effects of p32 are in agreement with studies on the role of p32 in yeast metabolism, which show that the p32 homologue is necessary for the maintenance of a normal level of OXPHOS (48). As in yeast, p32 has a profound

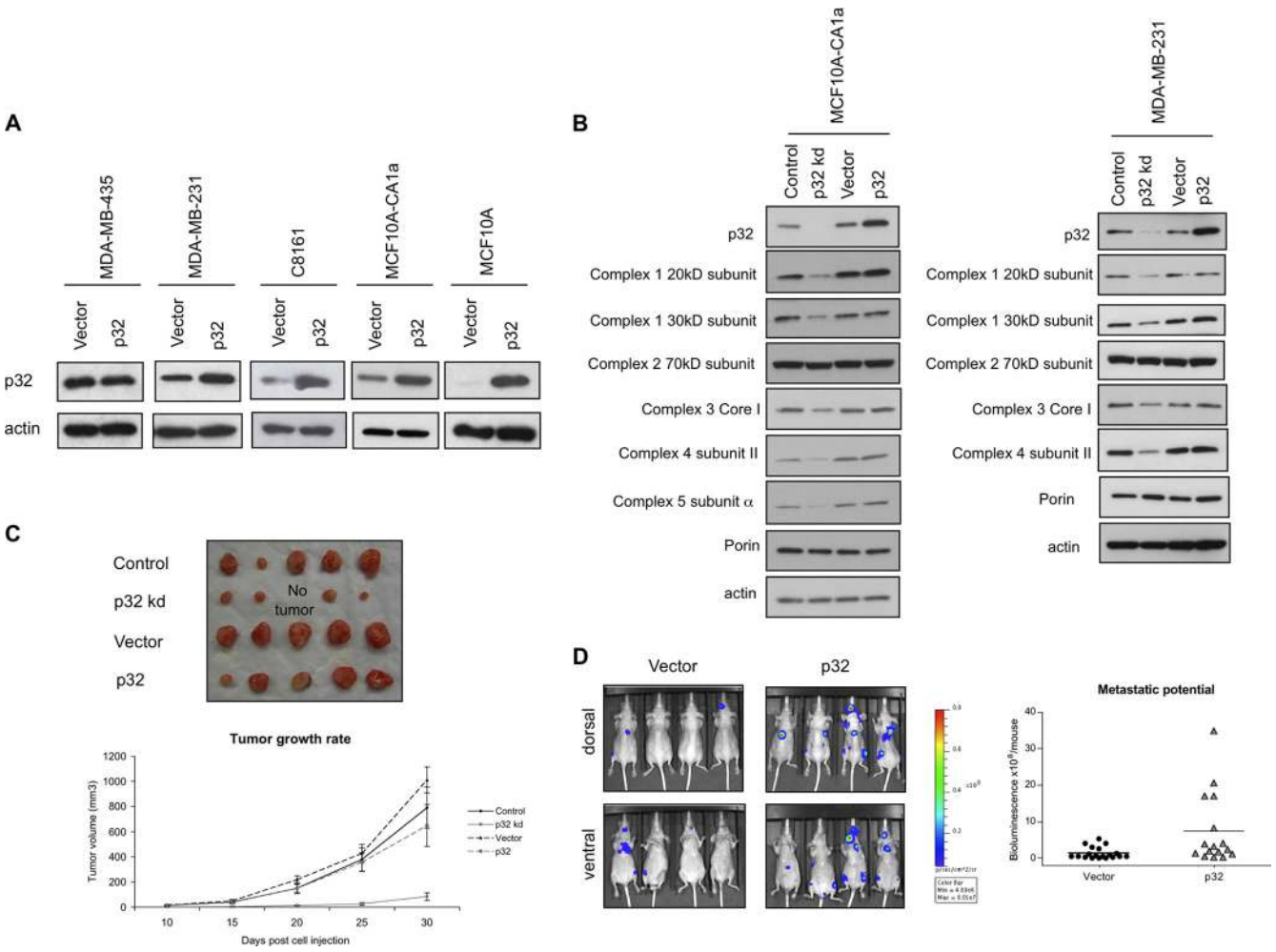

FIG. 10. Tumor growth properties and metastatic potential of p32-overexpressing cells. (A) Production of cell lines stably overexpressing p32. The indicated cell lines were transfected with a p32 cDNA-containing vector or an empty vector. MDA-MB-435 cells, which contain the highest levels of endogenous p32 among the cell lines tested, yielded no cultures with stable expression of p32 above the endogenous basal level. (B) Overexpression of p32 does not affect the expression levels of OXPHOS proteins. (C) Macroscopic appearance and volumes as a function of time of MDA-MB-231-luc-D3H2LN tumors derived from cells which stably express control or p32 shRNA or empty vector or p32 cDNA. P was <0.001 (control versus p32 kd tumors). (D) Metastatic potential of MDA-MB-231-luc-D3H2LN vector/p32 cells. (Left) Bioluminescence imaging of intracardially injected, luciferase-expressing MDA-MB-231 D3H2LN cells. Results were obtained 4 weeks after injection. Data depicted were derived from 3 independent experiments using at least 5 animals for each cell line injected. P was <0.05.

effect on tumor cell metabolism: knocking down p32 expression in cancer cells shifted the metabolism of the cells from OXPHOS to glycolysis, which was accompanied by an increase in lactate production and elevated glucose consumption. The p32 protein becomes extremely unstable when it is unable to localize to the mitochondria. This biological limitation thus rules out the possibility of clearly excluding the extramitochondrial functions of p32 from the regulation of tumor metabolism. Also, gene array analysis using control versus p32 knockdown cell lines did not reveal different gene signatures in the p32 knockdown cells that could readily explain the metabolic phenotypes we observed (data not shown). It is thus unlikely that extramitochondrial functions related to gene expression might have indirectly affected the mitochondrial metabolism of p32 knockdown cells.

The mammalian p32 protein may not be a general requirement for mammalian cells, as some normal cells show very low or undetectable expression of p32 (19, 59). Also, p32 overexpression is common in breast cancers but rare or nonexistent in some other malignant tissues, such as prostate carcinomas (19, 59).

The Warburg effect, evidenced by high aerobic glycolysis in tumors, is an almost universal feature of malignancy and is thought to provide a growth advantage to tumors (70). Our results are not easily reconciled with the hypothesis that the glycolytic phenotype is advantageous to tumor growth. If the Warburg effect confers a growth advantage, why would tumor cells upregulate a protein that counteracts this effect and why do the highly glycolytic cells produced by knocking down p32 grow poorly and show impaired tumorigenicity?

It has been proposed that the change to glycolysis is an adaptation to hypoxic conditions encountered by premalignant lesions during their initial growth, which takes the newly added cells farther away from the blood supply than their normal

counterpart cells (22). However, cells transformed *in vitro* also become glycolytic (2, 55), and some oncogenes, such as the c-Myc and Akt genes, enhance the expression of enzymes in the glycolytic pathway, promoting aerobic glycolysis (15, 50, 63). Perhaps the glycolytic phenotype is a side product of malignant transformation that, depending on circumstances such as the positioning of a cell within a tumor, can confer a growth and/or survival advantage or conversely be disadvantageous. In this regard, a recent study suggests that tumors form a symbiotic environment. This environment consists of cells in hypoxic regions, which need the glycolytic pathway to produce ATP, and cells in the well-oxygenated regions, which use the lactic acid from the hypoxic cells in OXPHOS (64). If this were the case, one would expect p32 expression to be the strongest outside the hypoxic regions within tumors. However, our results show that the opposite is true, i.e., that p32 expression is strongest in the hypoxic regions (19, 38), suggesting that p32 moderates glycolytic tendencies in these regions. However, we cannot exclude the possibility of a symbiotic relationship between cells that favor glycolysis and those that favor OXPHOS at the local microenvironment level.

The high rate of glycolytic metabolism in tumors was initially believed to result from impaired ability of cancer cells to carry out oxidative phosphorylation. However, this view has been challenged thorough the years and needs to be reappraised. In fact, defects in oxidative metabolism were not found in several highly proliferative tumor cell lines (47), and transformation of mesenchymal stem cells was shown to increase cell dependency on oxidative phosphorylation (20). Furthermore, that mitochondrial OXPHOS function might still be advantageous in highly glycolytic tumor cells is suggested by the facts that recycling of lactate via oxidative metabolism appears to be critical for tumorigenesis (64) and that oncogenes known to promote the use of the glycolytic pathway by tumors can also upregulate genes important for mitochondrial physiology and increase mitochondrial metabolism (13, 40, 66). More recently, it has been shown that mitochondrial STAT3 contributes to Ras-dependent malignant transformation via augmenting electron transport chain activity (26). Altogether, these findings suggest that oncogene-driven glycolytic metabolism should be balanced at least in part by concomitant changes to mitochondria. In view of this, one could hypothesize that the overexpression of proteins such as p32 is required to counteract the otherwise detrimental activity of an oncogene. It is noteworthy that c-Myc changes are common in breast cancers (41), which exhibit high glycolytic activity (29). We and others found that breast cancers and some other adenocarcinomas upregulate p32 while others, notably prostate cancer, do not (19, 59). Interestingly, a majority of prostate cancers, in contrast to many other malignancies, are not highly glycolytic (43). Thus, p32 may counteract the proglycolytic functions of c-Myc, while allowing its tumor-promoting effects to remain intact. In support of this model, database analysis shows that the p32 gene is a direct c-Myc target gene (Myc target database [77] at www.myc-cancer-gene.org).

In addition to increasing the expression of numerous enzymes in the glycolytic cascade, c-Myc has recently been shown to promote the use of glutamine (21, 72). Glutaminolysis is important not only for energy production but also for replenishing, through a process termed anapleurosis, the TCA cycle intermediates that are necessary precursors for the anabolic processes required for cancer cell growth (11, 18). Recently, coordination between glucose and glutamine utilization pathways has been described, and it has been suggested that this represents a metabolic checkpoint in highly glycolytic tumor cells (34). In view of this, it is possible to speculate that p32 has a role in mediating glutamine metabolism downstream of Myc.

Tumor cells depend on the expression of the oncogenes that contributed to their transformation. This is the case even if several oncogenes with redundant activities have become mutated in the same tumor cell; eliminating just one of the oncogenes induces cell death. This phenomenon is referred to as "oncogene addiction" (71). Perhaps a similar situation exists in tumor cell energy metabolism. Whether the Warburg effect is advantageous or not, a tumor cell cannot handle a drastic change in either direction from the metabolic balance that has developed during the tumorigenesis process. Existing data supporting this concept by Fantin et al. (16) showed that suppressing one of the glycolytic enzymes, lactate dehydrogenase A, reduced tumor growth, whereas our results show that enhancing glycolysis produces the same effect. Moreover, it has been reported that the expression of the glycolytic enzyme PKM2 is required for the shift in cellular metabolism to aerobic glycolysis and for tumor growth (9, 17). Tumor maintenance and malignancy of the cancer cell lines used in this study depend on mitochondrial oxidative phosphorylation via p32, despite the fact that these cells express PKM2. Finally, while we were able to restore p32 expression to the original level in p32 knockdown cells using forced expression of p32, we had difficulties deriving MDA-MB-435 cell lines overexpressing p32. Interestingly, in MDA-MB-435 cells the basal level of p32 expression was the highest among the various tumor cell lines we tested (19). This result suggests that shifting the balance too far toward OXPHOS is also detrimental, even under well-oxygenated cell culture conditions.

The expression of p32 is upregulated in tumors, particularly in breast cancers, and cell surface-expressed p32 is a tumor marker (19). Peptides and antibodies that bind to p32 specifically home to tumors and have been used to deliver nanoparticles and nanoparticle-embedded drugs to tumors, particularly to the regions in tumors that are poorly served by blood vessels (19, 35, 38, 69). Moreover, a p32-binding peptide has an inherent antitumor activity (38). The present results show that reducing p32 expression in tumor cells suppresses tumor growth. Thus, p32 is not only an important regulator of tumor metabolism but also a promising molecular target in tumor diagnosis and therapy.

ACKNOWLEDGMENTS

We thank Mark Wade for helpful suggestions, Lianglin Zhang for his initial involvement on the project, Kazuki N. Sugahara for intracardiac injections, and Yeun Su Choo for advice on mitochondrial assays. Khatereh Motamedchaboki (Burnham Institute Proteomics facility) carried out the mass spectrometry analysis, and Alexey Eroshkin (Burnham Institute Bioinformatics Shared Resource) performed the bioinformatics phylogenic analysis. Sarah E. Calvo kindly provided the phylogenic matrix of the mouse MitoCarta genes.

This work was supported by grants W81XWH-08-1-0727 from the Department of Defense Breast Cancer Research Program and CA115410 and in part by CA104898 and Cancer Center Support Grant CA 30199 from the NCI. V.F. received support from the Susan Komen Foundation.

REFERENCES

1. **Alirol, E., and J. C. Martinou.** 2006. Mitochondria and cancer: is there a morphological connection? Oncogene **25:**4706–4716.
2. **Biaglow, J. E., G. Cerniglia, S. Tuttle, V. Bakanauskas, C. Stevens, and G. McKenna.** 1997. Effect of oncogene transformation of rat embryo cells on cellular oxygen consumption and glycolysis. Biochem. Biophys. Res. Commun. **235:**739–742.
3. **Brill, L. M., K. Motamedchaboki, S. Wu, and D. A. Wolf.** 2009. Comprehensive proteomic analysis of Schizosaccharomyces pombe by two-dimensional HPLC-tandem mass spectrometry. Methods **48:**311–319.
4. **Caraux, G., and S. Pinloche.** 2005. PermutMatrix: a graphical environment to arrange gene expression profiles in optimal linear order. Bioinformatics **21:**1280–1281.
5. **Cavalli, L. R., M. Varella-Garcia, and B. C. Liang.** 1997. Diminished tumorigenic phenotype after depletion of mitochondrial DNA. Cell Growth Differ. **8:**1189–1198.
6. **Cavdar Koc, E., A. Ranasinghe, W. Burkhart, K. Blackburn, H. Koc, A. Moseley, and L. L. Spremulli.** 2001. A new face on apoptosis: death-associated protein 3 and PDCD9 are mitochondrial ribosomal proteins. FEBS Lett. **492:**166–170.
7. **Chen, Y. B., C. T. Jiang, G. Q. Zhang, J. S. Wang, and D. Pang.** 2009. Increased expression of hyaluronic acid binding protein 1 is correlated with poor prognosis in patients with breast cancer. J. Surg. Oncol. **100:**382–386.
8. **Christian, S., J. Pilch, M. E. Akerman, K. Porkka, P. Laakkonen, and E. Ruoslahti.** 2003. Nucleolin expressed at the cell surface is a marker of endothelial cells in angiogenic blood vessels. J. Cell Biol. **163:**871–878.
9. **Christofk, H. R., M. G. Vander Heiden, M. H. Harris, A. Ramanathan, R. E. Gerszten, R. Wei, M. D. Fleming, S. L. Schreiber, and L. C. Cantley.** 2008. The M2 splice isoform of pyruvate kinase is important for cancer metabolism and tumour growth. Nature **452:**230–233.
10. **Deb, T. B., and K. Datta.** 1996. Molecular cloning of human fibroblast hyaluronic acid-binding protein confirms its identity with P-32, a protein co-purified with splicing factor SF2. J. Biol. Chem. **271:**2206–2212.
11. **DeBerardinis, R. J., A. Mancuso, E. Daikhin, I. Nissim, M. Yudkoff, S. Wehrli, and C. B. Thompson.** 2007. Beyond aerobic glycolysis: transformed cells can engage in glutamine metabolism that exceeds the requirement for protein and nucleotide synthesis. Proc. Natl. Acad. Sci. U. S. A. **104:**19345–19350.
12. **Dedio, J., W. Jahnen-Dechent, M. Bachmann, and W. Muller-Esterl.** 1998. The multiligand-binding protein gC1qR, putative C1q receptor, is a mitochondrial protein. J. Immunol. **160:**3534–3542.
13. **Dejean, L., B. Beauvoit, O. Bunoust, B. Guerin, and M. Rigoulet.** 2002. Activation of Ras cascade increases the mitochondrial enzyme content of respiratory competent yeast. Biochem. Biophys. Res. Commun. **293:**1383–1388.
14. **Dias, N., and C. Bailly.** 2005. Drugs targeting mitochondrial functions to control tumor cell growth. Biochem. Pharmacol. **70:**1–12.
15. **Elstrom, R. L., D. E. Bauer, M. Buzzai, R. Karnauskas, M. H. Harris, D. R. Plas, H. Zhuang, R. M. Cinalli, A. Alavi, C. M. Rudin, and C. B. Thompson.** 2004. Akt stimulates aerobic glycolysis in cancer cells. Cancer Res. **64:**3892–3899.
16. **Fantin, V. R., J. St-Pierre, and P. Leder.** 2006. Attenuation of LDH-A expression uncovers a link between glycolysis, mitochondrial physiology, and tumor maintenance. Cancer Cell **9:**425–434.
17. **Ferguson, E. C., and J. C. Rathmell.** 2008. New roles for pyruvate kinase M2: working out the Warburg effect. Trends Biochem. Sci. **33:**359–362.
18. **Feron, O.** 2009. Pyruvate into lactate and back: from the Warburg effect to symbiotic energy fuel exchange in cancer cells. Radiother. Oncol. **92:**329–333.
19. **Fogal, V., L. Zhang, S. Krajewski, and E. Ruoslahti.** 2008. Mitochondrial/cell-surface protein p32/gC1qR as a molecular target in tumor cells and tumor stroma. Cancer Res. **68:**7210–7218.
20. **Funes, J. M., M. Quintero, S. Henderson, D. Martinez, U. Qureshi, C. Westwood, M. O. Clements, D. Bourboulia, R. B. Pedley, S. Moncada, and C. Boshoff.** 2007. Transformation of human mesenchymal stem cells increases their dependency on oxidative phosphorylation for energy production. Proc. Natl. Acad. Sci. U. S. A. **104:**6223–6228.
21. **Gao, P., I. Tchernyshyov, T. C. Chang, Y. S. Lee, K. Kita, T. Ochi, K. I. Zeller, A. M. De Marzo, J. E. Van Eyk, J. T. Mendell, and C. V. Dang.** 2009. c-Myc suppression of miR-23a/b enhances mitochondrial glutaminase expression and glutamine metabolism. Nature **458:**762–765.
22. **Gatenby, R. A., and R. J. Gillies.** 2004. Why do cancers have high aerobic glycolysis? Nat. Rev. Cancer **4:**891–899.
23. **Ghebrehiwet, B., B. L. Lim, E. I. Peerschke, A. C. Willis, and K. B. Reid.** 1994. Isolation, cDNA cloning, and overexpression of a 33-kD cell surface glycoprotein that binds to the globular "heads" of C1q. J. Exp. Med. **179:**1809–1821.
24. **Ghebrehiwet, B., and E. I. Peerschke.** 2004. cC1q-R (calreticulin) and gC1q-R/p33: ubiquitously expressed multi-ligand binding cellular proteins involved in inflammation and infection. Mol. Immunol. **41:**173–183.
25. **Ghosh, I., A. R. Chowdhury, M. R. Rajeswari, and K. Datta.** 2004. Differential expression of hyaluronic acid binding protein 1 (HABP1)/P32/C1QBP during progression of epidermal carcinoma. Mol. Cell. Biochem. **267:**133–139.
26. **Gough, D. J., A. Corlett, K. Schlessinger, J. Wegrzyn, A. C. Larner, and D. E. Levy.** 2009. Mitochondrial STAT3 supports Ras-dependent oncogenic transformation. Science **324:**1713–1716.
27. **Guarino, R. D., L. E. Dike, T. A. Haq, J. A. Rowley, J. B. Pitner, and M. R. Timmins.** 2004. Method for determining oxygen consumption rates of static cultures from microplate measurements of pericellular dissolved oxygen concentration. Biotechnol. Bioeng. **86:**775–787.
28. **Herwald, H., J. Dedio, R. Kellner, M. Loos, and W. Muller-Esterl.** 1996. Isolation and characterization of the kininogen-binding protein p33 from endothelial cells. Identity with the gC1q receptor. J. Biol. Chem. **271:**13040–13047.
29. **Isidoro, A., E. Casado, A. Redondo, P. Acebo, E. Espinosa, A. M. Alonso, P. Cejas, D. Hardisson, J. A. Fresno Vara, C. Belda-Iniesta, M. Gonzalez-Baron, and J. M. Cuezva.** 2005. Breast carcinomas fulfill the Warburg hypothesis and provide metabolic markers of cancer prognosis. Carcinogenesis **26:**2095–2104.
30. **Itahana, K., and Y. Zhang.** 2008. Mitochondrial p32 is a critical mediator of ARF-induced apoptosis. Cancer Cell **13:**542–553.
31. **Jin, S.** 2006. Autophagy, mitochondrial quality control, and oncogenesis. Autophagy **2:**80–84.
32. **Jinwook Seo, B. S.** 2002. Interactively exploring hierarchical clustering results. IEEE Comput. **35:**80–86.
33. **Joseph, K., Y. Shibayama, Y. Nakazawa, E. I. Peerschke, B. Ghebrehiwet, and A. P. Kaplan.** 1999. Interaction of factor XII and high molecular weight kininogen with cytokeratin 1 and gC1qR of vascular endothelial cells and with aggregated Abeta protein of Alzheimer's disease. Immunopharmacology **43:**203–210.
34. **Kaadige, M. R., R. E. Looper, S. Kamalanaadhan, and D. E. Ayer.** 2009. Glutamine-dependent anapleurosis dictates glucose uptake and cell growth by regulating MondoA transcriptional activity. Proc. Natl. Acad. Sci. U. S. A. **106:**14878–14883.
35. **Karmali, P. P., V. R. Kotamraju, M. Kastantin, M. Black, D. Missirlis, M. Tirrell, and E. Ruoslahti.** 2009. Targeting of albumin-embedded paclitaxel nanoparticles to tumors. Nanomedicine **5:**73–82.
36. **Kim, H. R., H. J. Chae, M. Thomas, T. Miyazaki, A. Monosov, E. Monosov, M. Krajewska, S. Krajewski, and J. C. Reed.** 2007. Mammalian dap3 is an essential gene required for mitochondrial homeostasis in vivo and contributing to the extrinsic pathway for apoptosis. FASEB J. **21:**188–196.
37. **Krainer, A. R., A. Mayeda, D. Kozak, and G. Binns.** 1991. Functional expression of cloned human splicing factor SF2: homology to RNA-binding proteins, U1 70K, and Drosophila splicing regulators. Cell **66:**383–394.
38. **Laakkonen, P., M. E. Akerman, H. Biliran, M. Yang, F. Ferrer, T. Karpanen, R. M. Hoffman, and E. Ruoslahti.** 2004. Antitumor activity of a homing peptide that targets tumor lymphatics and tumor cells. Proc. Natl. Acad. Sci. U. S. A. **101:**9381–9386.
39. **Lawrence, J. W., S. Darkin-Rattray, F. Xie, A. H. Neims, and T. C. Rowe.** 1993. 4-Quinolones cause a selective loss of mitochondrial DNA from mouse L1210 leukemia cells. J. Cell. Biochem. **51:**165–174.
40. **Li, F., Y. Wang, K. I. Zeller, J. J. Potter, D. R. Wonsey, K. A. O'Donnell, J. W. Kim, J. T. Yustein, L. A. Lee, and C. V. Dang.** 2005. Myc stimulates nuclearly encoded mitochondrial genes and mitochondrial biogenesis. Mol. Cell. Biol. **25:**6225–6234.
41. **Liao, D. J., and R. B. Dickson.** 2000. c-Myc in breast cancer. Endocr. Relat. Cancer **7:**143–164.
42. **Lim, B. L., K. B. Reid, B. Ghebrehiwet, E. I. Peerschke, L. A. Leigh, and K. T. Preissner.** 1996. The binding protein for globular heads of complement C1q, gC1qR. Functional expression and characterization as a novel vitronectin binding factor. J. Biol. Chem. **271:**26739–26744.
43. **Liu, Y.** 2006. Fatty acid oxidation is a dominant bioenergetic pathway in prostate cancer. Prostate Cancer Prostatic Dis. **9:**230–234.
44. **Lum, J. J., R. J. DeBerardinis, and C. B. Thompson.** 2005. Autophagy in metazoans: cell survival in the land of plenty. Nat. Rev. Mol. Cell Biol. **6:**439–448.
45. **Mariani, L., C. Beaudry, W. S. McDonough, D. B. Hoelzinger, E. Kaczmarek, F. Ponce, S. W. Coons, A. Giese, R. W. Seiler, and M. E. Berens.** 2001. Death-associated protein 3 (Dap-3) is overexpressed in invasive glioblastoma cells in vivo and in glioma cell lines with induced motility phenotype in vitro. Clin. Cancer Res. **7:**2480–2489.
46. **Matthews, D. A., and W. C. Russell.** 1998. Adenovirus core protein V interacts with p32—a protein which is associated with both the mitochondria and the nucleus. J. Gen. Virol. **79:**1677–1685.
47. **Moreno-Sanchez, R., S. Rodriguez-Enriquez, A. Marin-Hernandez, and E. Saavedra.** 2007. Energy metabolism in tumor cells. FEBS J. **274:**1393–1418.
48. **Muta, T., D. Kang, S. Kitajima, T. Fujiwara, and N. Hamasaki.** 1997. p32 protein, a splicing factor 2-associated protein, is localized in mitochondrial matrix and is functionally important in maintaining oxidative phosphorylation. J. Biol. Chem. **272:**24363–24370.
49. **Oh, P., Y. Li, J. Yu, E. Durr, K. M. Krasinska, L. A. Carver, J. E. Testa, and J. E. Schnitzer.** 2004. Subtractive proteomic mapping of the endothelial

surface in lung and solid tumours for tissue-specific therapy. Nature **429:** 629–635.
50. **Osthus, R. C., H. Shim, S. Kim, Q. Li, R. Reddy, M. Mukherjee, Y. Xu, D. Wonsey, L. A. Lee, and C. V. Dang.** 2000. Deregulation of glucose transporter 1 and glycolytic gene expression by c-Myc. J. Biol. Chem. **275:**21797–21800.
51. **Pagliarini, D. J., S. E. Calvo, B. Chang, S. A. Sheth, S. B. Vafai, S. E. Ong, G. A. Walford, C. Sugiana, A. Boneh, W. K. Chen, D. E. Hill, M. Vidal, J. G. Evans, D. R. Thorburn, S. A. Carr, and V. K. Mootha.** 2008. A mitochondrial protein compendium elucidates complex I disease biology. Cell **134:**112–123.
52. **Parle-McDermott, A., P. McWilliam, O. Tighe, D. Dunican, and D. T. Croke.** 2000. Serial analysis of gene expression identifies putative metastasis-associated transcripts in colon tumour cell lines. Br. J. Cancer **83:**725–728.
53. **Peerschke, E. I., and B. Ghebrehiwet.** 2007. The contribution of gC1qR/p33 in infection and inflammation. Immunobiology **212:**333–342.
54. **Pellegrini, M., E. M. Marcotte, M. J. Thompson, D. Eisenberg, and T. O. Yeates.** 1999. Assigning protein functions by comparative genome analysis: protein phylogenetic profiles. Proc. Natl. Acad. Sci. U. S. A. **96:**4285–4288.
55. **Ramanathan, A., C. Wang, and S. L. Schreiber.** 2005. Perturbational profiling of a cell-line model of tumorigenesis by using metabolic measurements. Proc. Natl. Acad. Sci. U. S. A. **102:**5992–5997.
56. **Reef, S., O. Shifman, M. Oren, and A. Kimchi.** 2007. The autophagic inducer smARF interacts with and is stabilized by the mitochondrial p32 protein. Oncogene **26:**6677–6683.
57. **Reef, S., E. Zalckvar, O. Shifman, S. Bialik, H. Sabanay, M. Oren, and A. Kimchi.** 2006. A short mitochondrial form of p19ARF induces autophagy and caspase-independent cell death. Mol. Cell **22:**463–475.
58. **Rozanov, D. V., B. Ghebrehiwet, B. Ratnikov, E. Z. Monosov, E. I. Deryugina, and A. Y. Strongin.** 2002. The cytoplasmic tail peptide sequence of membrane type-1 matrix metalloproteinase (MT1-MMP) directly binds to gC1qR, a compartment-specific chaperone-like regulatory protein. FEBS Lett. **527:**51–57.
59. **Rubinstein, D. B., A. Stortchevoi, M. Boosalis, R. Ashfaq, B. Ghebrehiwet, E. I. Peerschke, F. Calvo, and T. Guillaume.** 2004. Receptor for the globular heads of C1q (gC1q-R, p33, hyaluronan-binding protein) is preferentially expressed by adenocarcinoma cells. Int. J. Cancer **110:**741–750.
60. **Ruoslahti, E.** 2004. Vascular zip codes in angiogenesis and metastasis. Biochem. Soc. Trans. **32:**397–402.
61. **Santner, S. J., P. J. Dawson, L. Tait, H. D. Soule, J. Eliason, A. N. Mohamed, S. R. Wolman, G. H. Heppner, and F. R. Miller.** 2001. Malignant MCF10CA1 cell lines derived from premalignant human breast epithelial MCF10AT cells. Breast Cancer Res. Treat. **65:**101–110.
62. **Shaw, R. J.** 2006. Glucose metabolism and cancer. Curr. Opin. Cell Biol. **18:**598–608.
63. **Shim, H., C. Dolde, B. C. Lewis, C. S. Wu, G. Dang, R. A. Jungmann, R. Dalla-Favera, and C. V. Dang.** 1997. c-Myc transactivation of LDH-A: implications for tumor metabolism and growth. Proc. Natl. Acad. Sci. U. S. A. **94:**6658–6663.
64. **Sonveaux, P., F. Vegran, T. Schroeder, M. C. Wergin, J. Verrax, Z. N. Rabbani, C. J. De Saedeleer, K. M. Kennedy, C. Diepart, B. F. Jordan, M. J. Kelley, B. Gallez, M. L. Wahl, O. Feron, and M. W. Dewhirst.** 2008. Targeting lactate-fueled respiration selectively kills hypoxic tumor cells in mice. J. Clin. Invest. **118:**3930–3942.
65. **Storz, P., A. Hausser, G. Link, J. Dedio, B. Ghebrehiwet, K. Pfizenmaier, and F. J. Johannes.** 2000. Protein kinase C [micro] is regulated by the multifunctional chaperon protein p32. J. Biol. Chem. **275:**24601–24607.
66. **Telang, S., A. N. Lane, K. K. Nelson, S. Arumugam, and J. Chesney.** 2007. The oncoprotein H-RasV12 increases mitochondrial metabolism. Mol. Cancer **6:**77.
67. **Timmer, J. C., M. Enoksson, E. Wildfang, W. Zhu, Y. Igarashi, J. B. Denault, Y. Ma, B. Dummitt, Y. H. Chang, A. E. Mast, A. Eroshkin, J. W. Smith, W. A. Tao, and G. S. Salvesen.** 2007. Profiling constitutive proteolytic events in vivo. Biochem. J. **407:**41–48.
68. **van den Bogert, C., B. H. Dontje, M. Holtrop, T. E. Melis, J. C. Romijn, J. W. van Dongen, and A. M. Kroon.** 1986. Arrest of the proliferation of renal and prostate carcinomas of human origin by inhibition of mitochondrial protein synthesis. Cancer Res. **46:**3283–3289.
69. **von Maltzahn, G., Y. Ren, J. H. Park, D. H. Min, V. R. Kotamraju, J. Jayakumar, V. Fogal, M. J. Sailor, E. Ruoslahti, and S. N. Bhatia.** 2008. In vivo tumor cell targeting with"click" nanoparticles. Bioconjug. Chem. **19:** 1570–1578.
70. **Warburg, O.** 1956. On the origin of cancer cells. Science **123:**309–314.
71. **Weinstein, I. B.** 2002. Cancer addiction to oncogenes—the Achilles heal of cancer. Science **297:**63–64.
72. **Wise, D. R., R. J. DeBerardinis, A. Mancuso, N. Sayed, X. Y. Zhang, H. K. Pfeiffer, I. Nissim, E. Daikhin, M. Yudkoff, S. B. McMahon, and C. B. Thompson.** 2008. Myc regulates a transcriptional program that stimulates mitochondrial glutaminolysis and leads to glutamine addiction. Proc. Natl. Acad. Sci. U. S. A. **105:**18782–18787.
73. **Wiseman, A., and G. Attardi.** 1978. Reversible tenfold reduction in mitochondria DNA content of human cells treated with ethidium bromide. Mol. Gen. Genet. **167:**51–63.
74. **Wittig, I., H. P. Braun, and H. Schagger.** 2006. Blue native PAGE. Nat. Protoc. **1:**418–428.
75. **Yang, C., A. D. Richardson, A. Osterman, and J. W. Smith.** 2008. Profiling of central metabolism in human cancer cells by two-dimensional NMR, GC-MS analysis, and isotopomer modeling. Metabolomics **4:**13–29.
76. **Yu, M., Y. Shi, X. Wei, Y. Yang, Y. Zhou, X. Hao, N. Zhang, and R. Niu.** 2007. Depletion of mitochondrial DNA by ethidium bromide treatment inhibits the proliferation and tumorigenesis of T47D human breast cancer cells. Toxicol. Lett. **170:**83–93.
77. **Zeller, K. I., A. G. Jegga, B. J. Aronow, K. A. O'Donnell, and C. V. Dang.** 2003. An integrated database of genes responsive to the Myc oncogenic transcription factor: identification of direct genomic targets. Genome Biol. **4:**R69.